Submitted to *ApJ.*, 2006 Jan. 25; Accepted 2006 April 10

A Model for Spectral and Compositional Variability at High Energies in Large, Gradual Solar Particle Events

Allan J. Tylka

E.O. Hulburt Center for Space Research, Code 7652, Naval Research Laboratory, Washington, DC 20375; allan.tylka@nrl.navy.mil

and

Martin A. Lee

Space Science Center and Institute for the Study of Earth, Oceans, and Space, University of New Hampshire, Durham, NH 03824-3525; marty.lee@unh.edu

ABSTRACT

A cogent preponderance of evidence points to shocks driven by fast coronal mass ejections (CMEs) as the dominant accelerators in large, gradual solar energetic particle (SEP) events. At energies above a few tens of MeV per nucleon, these events are highly variable in their spectral characteristics, elemental composition, and mean ionic charge states. Moreover, there are high degrees of correlation among these variable factors. A detailed explanation of how shock acceleration can give rise to these patterns of variability is therefore a critical challenge. We have recently proposed that this variability results from the interplay of two factors: evolution in the geometry of the CME-driven shock as it moves outward from the Sun; and a compound seed population, typically comprising at least suprathermals from the corona (or solar wind) and suprathermals from flares. In this paper we present a simple analytical implementation of these ideas. The resulting calculations semi-quantitatively reproduce many key features of the observed SEP variability, including spectral morphologies and energy dependence in Fe/O, ^{3}He/^{4}He, and mean ionic charges, in ways that are consistent with the correlations found in the data. The model also makes a quantitative prediction for the average high-energy Fe/O enhancement in Fe-rich gradual events that is borne out by thirty years of data. The model further provides a quantitative explanation for the Breneman & Stone fractionation effect, a basic feature of SEP phenomenology that has been known for twenty years but which heretofore

has gone unexplained. These calculations must be bolstered by future efforts, in which these ideas are embedded in realistic CME-shock simulations and coupled to rigorous treatments of particle transport. The calculations also leave specific issues, such as suprathermal densities in the corona and refinements of our understanding of the injection process at shocks of arbitrary obliquity, open for future theoretical and observational investigations. Nevertheless, these first results are sufficient to suggest that we have found a comprehensive framework for understanding the complexity of high-energy variability in terms of shock physics for most, if not all, large SEP events.

Subject headings: acceleration of particles – shock waves -- Sun: particle emission – coronal mass ejections — flares

1. Introduction

A large body of observations in the 1980s led to the formulation of a "standard model", by which solar energetic particle (SEP) events are divided into two categories, "gradual" and "impulsive" (Reames 1995a, 1999). These names are short-hand for the likely sites and mechanisms of particle acceleration. Gradual events, which are the focus of this paper, are those in which the overwhelming preponderance of evidence points to acceleration at shocks driven by fast coronal mass ejections (CMEs). Impulsive events, on the other hand, are generally ascribed to particle acceleration at sites associated with flares, probably through resonant wave-particle interactions following magnetic reconnection (Reames 2002; Wang et al. 2006). The two types of events differ in their typical sizes (with gradual events yielding much larger particle intensities and fluences) and in the spatial distribution of their source regions (with impulsive events originating from a comparatively narrow range of solar longitudes that are magnetically well-connected to the observer). At energies of a few MeV/nucleon, the two types of events can also be distinguished by compositional signatures, most notably with impulsive events showing enhanced Fe/O and ^{3}He/^{4}He ratios and higher mean ionic charges, especially for Fe. More recently, the compositional distinction between impulsive and gradual events has been reinforced by the first systematic survey of energetic ions at ∼3-10 MeV/nucleon from the upper two-thirds of the periodic table (Reames 2000; Reames & Ng 2004; see also Mason et al. 2004). Whereas gradual events have ultra-heavy abundances that are consistent with nominal coronal values, impulsive events show ∼100-1000-fold enhancements, thereby continuing the systematic trend by which enhancements become larger as mass increases.

But when we examine large gradual events at energies above the few MeV/nucleon

where the two categories were originally developed, at least some of the compositional distinctions between the two event types become blurred: some large gradual events show Fe/O and ^{3}He/^{4}He ratios and mean Fe charge values ($<Q_{Fe}>$) close to those typically associated with impulsive events. This blurring has generally been the primary factor behind questions to the validity of the two-class paradigm. Other factors contributing to this notion of blurred distinctions include (1) a wider dynamic range of measureable ^{3}He/^{4}He ratios in both impulsive and gradual events (Mason et al. 1999; 2002), made possible by the better isotopic resolution and increased collecting power in the new particle instruments; and (2) the discovery of generally smaller and slower CMEs that sometimes accompany impulsive SEP events (Kahler et al. 2001).

However, focus on this ostensible "blurring" understates the true extent of the challenge to our understanding of the origins of SEPs. In fact, as we move to higher energies, the larger and more compelling problem is the dramatic event-to-event variability. Various features of this variability, which were only glimpsed in Solar Cycles 21 and 22 (Mazur et al. 1992; Tylka & Dietrich 1999), have now been clearly defined by the precise and comprehensive measurements of many SEP events from *Wind*, the *Advanced Composition Explorer (ACE)*, the *Solar and Heliospheric Observatory (SOHO)*, and other satellites in Cycle 23 (Cane et al. 2003; Cohen et al. 1999a, 1999b, 2003, 2005; Mäkelä & Torsti 2001; Mewaldt et al. 2005; Reames et al. 2001; Reames & Ng 2004; Torsti et al. 2000; Tylka 2001; Tylka et al. 2000, 2001, 2002, 2005, 2006). For example, gradual events show event-integrated Fe/O values that vary by roughly an order of magnitude at ∼5 MeV/nucleon. But at ∼50 MeV/nucleon, the variation in this same quantity spans nearly three orders of magnitude. This wider spread reflects the fact that in some events, iron has a harder energy spectrum than oxygen, while in others, the iron spectrum is much softer than the oxygen spectrum. There are also clear qualitative differences in the character of the energy spectra: in some events, the spectral shapes are well fit by power-laws from a few MeV/nucleon out to the highest measureable energies. In other events, the spectra are power-laws modulated at high energy by exponential rollovers.

A better statement of the fundamental challenge to the "standard model" is therefore the following: can we find a comprehensive and quantitative understanding of this high-energy variability within the context of shock acceleration? Or is the observed variability so complex that something other than shock acceleration must be responsible for the high energy particles in some events? Answers to these questions have potentially significant import, both for our basic understanding of particle acceleration in astrophysical plasmas and for current efforts to develop predictive capabilities for the SEP radiation hazards facing future manned and robotic space-exploration missions.

Although the high-energy SEP variability is daunting, it also contains compelling clues that enable us to answer these questions. In particular, there are high levels of correlation among the various aspects of the high-energy variability. Power-law spectra are not observed at high energies in events in which the Fe/O ratio is highly suppressed with respect to the nominal coronal value; and events in which the high-energy Fe/O is strongly enhanced do not exhibit exponential rollovers. (See Tylka et al. 2005, Figure 9.) Similarly, $<Q_{Fe}>$ values above ∼30 MeV/nucleon range from ∼10 to ∼22. But we do not see high iron charge states when Fe/O is suppressed, nor do we see low Fe charge states when Fe/O is enhanced. (See Tylka et al. 2005, Figure 17.) These correlations among spectral shape, Fe/O, and charge states are powerful constraints for SEP models. The correct explanation is likely to be one in which these correlations arise in a natural fashion. Conversely, these strong correlations also imply that explanations that address these various features in a piece-meal fashion are unlikely to be adequate.

This paper is the third of a series on the problem of SEP variability at high energies. In the first paper (Tylka et al. 2005), we used observations from *ACE*, *Wind*, and *GOES* in the 43 largest events of 1997-2003 to illustrate systematic tendencies in the high-energy variability. This study motivated the hypothesis that the variability could be understood in terms of the interplay of seed populations and shock geometry. In the second paper (Tylka et al. 2006), we examined in detail two large events that exemplify the extremes of the variable behavior. In this paper, we present a simple analytical implementation of the shock geometry hypothesis. The reader is referred to the two earlier papers for observations to be compared with the calculations presented here. Preliminary reports on this model have been presented elsewhere (Tylka 2005; Tylka & Lee 2006).

2. Why does shock geometry matter?

Sarris & Krimigis (1985) made perhaps the first observation indicating that the quasi-perpendicular geometry is particularly effective in accelerating particles to high energies at traveling interplanetary shocks. Many authors (Jokipii 1982, 1987; Decker & Vlahos 1986; Ostrowski 1991; Webb et al. 1995; Giacalone 2005a,b) have examined this notion theoretically and found that acceleration time scales at quasi-perpendicular shocks can be orders of magnitude shorter than those of quasi-parallel shocks. This rapid acceleration rate is particularly important for high energy SEPs, since the maximum attainable energy generally decreases as the shock moves outward and the ambient magnetic field weakens. (See for example, Zank et al. 2000, Figure 7.) Figure 1 shows two recent theoretical estimates of the consequence of shock geometry for spectral shape. Lee (2005a) derived the explicit

dependence of the shock-accelerated spectrum's rollover energy on θ_{Bn}, the angle between the upstream magnetic field vector **B** and the shock normal **n**. Giacalone (2005a) obtained qualitatively similar spectra using numerical time-dependent test-particle simulations. These results imply that, if a shock takes on a range of θ_{Bn} values, the high energies will be dominated by particles produced when the shock was quasi-perpendicular.

We would generally expect the non-radial expansion of CMEs (e.g., Zhang et al. 2001) to produce extensive regions of quasi-perpendicular shocks on their flanks, at least out to altitudes of a few R_S. These quasi-perpendicular regions have previously been identified as a potential source of metric type-II radio emission (Steinolfson 1984). Recent precise studies of ground-level events (GLEs, Bieber et al. 2004; Sáiz et al. 2005) have shown that CMEs are typically at these altitudes when the highest-energy solar particles are released into interplanetary space.

Three-dimensional MHD simulations have recently been used to investigate the evolution of θ_{Bn} as a CME-driven shock moves outward from the Sun. Figure 2 shows results from Manchester et al. (2005). The two field lines considered here were at the same solar longitude, but at different latitudes. Along one field line, the shock initially broadsides the field line and is therefore nearly perpendicular. As the shock expands and envelopes the field line, θ_{Bn} decreases, falling to 10° by 20 R_S. However, on the other field line, the shock normal remains nearly parallel to the magnetic field along this whole distance. The shock-normal angles for both field lines increase far from the Sun and reach values near 45° at 1 AU because of the spiral nature of the interplanetary magnetic field. Of course, this later evolution is generally not relevant for high-energy SEPs.

The simulations in Figure 2 are not precisely what we need to address SEP observations. For one thing, the simulations do not trace the shock from $\sim$2 R_S, where SEP production apparently starts, at least in some events (Tylka et al. 2003; Mewaldt et al. 2003; Bieber et al. 2004; Tylka & Lee 2006). The calculations also employ a solar-minimum coronal model, far simpler than coronal configurations at solar maximum, when most SEPs are produced. Nevertheless these simulations, combined with injection altitudes inferred from recent SEP timing studies and the extensive body of theoretical work represented in Figure 1, make evolution in θ_{Bn} a strong and natural candidate for explaining SEP spectral variability.

But, as we have already discussed, high-energy spectral shape and composition are tied together. How can θ_{Bn} affect SEP composition? Figure 3 (from Tylka et al. 2005) sketches the potential connection. The seed population for shock-accelerated SEPs comprises both suprathermals from the corona (or solar wind, depending upon the location at which the acceleration occurs) and from flares. As noted in Figure 3, these two components have distinctive compositional characteristics. The flare ions in the seed population could be

either remnants from previous activity (Mason et al. 1999; Tylka et al. 2001) or come from the associated flare (Reames 2002; Li & Zank 2005) if open field lines connect the flare site to the shock front. Surveys of interplanetary ^{3}He/^{4}He (Richardson et al. 1990; Laivola et al. 2003; Torsti et al. 2003; Wiedenbeck et al. 2003), compared to the average solar-wind value (Gloeckler & Geiss 1998), suggest that flare suprathermals become more important at higher seed energies.

Under most conditions, efficient acceleration requires a higher initial speed at quasi-perpendicular shocks than at quasi-parallel shocks (Forman & Webb 1985; Jokipii 1987; Webb et al. 1995; Zank et al. 2004; but see Giacalone 2005a,b for a dissenting view.) Thus, as also sketched in Figure 3, flare suprathermals are more likely to provide the seed particles for quasi-perpendicular shocks. But as the shock moves outward and θ_{Bn} decreases, the spectra soften, while at the same time the injection threshold is lowered, so that the coronal component increasingly dominates the accessible seed population. The net effect of this evolution is to allow the unique characteristics of flare-suprathermals to be preferentially reflected among the higher-energy SEPs, causing Fe/O, $< Q_{Fe} >$, and ^{3}He/^{4}He to increase with energy. Of course, the relative sizes of the coronal and flare components in the seed population can vary from event to event. Moreover, as suggested by Figure 2, there can also be field lines along which the quasi-perpendicular phase is absent. In those cases, we might expect to see exponential rollovers within the energy range of our instruments, as well as charge states characteristic of the corona and/or solar-wind.

We now present a simple analytical implementation of this scenario.

3. An Analytical Implementation of the Shock-Geometry Hypothesis

To specify the differential intensity F_i of ion species i at non-relativistic energies, we generalize the functional form suggested by Ellison & Ramaty (1985) and write

$$F_i(E, \theta_{Bn}) = C_i E^{-\gamma} \exp(-E/E_{0i}), \tag{1}$$

where

$$E_{0i} = E_0 [Q_i/A_i][\sec \theta_{Bn}]^{2/(2\gamma-1)} \equiv \check{E}_{0i} [\sec \theta_{Bn}]^{2/(2\gamma-1)}. \tag{2}$$

E is the kinetic energy in MeV/nucleon, θ_{Bn} is the angle between the shock normal and the upstream magnetic field, Q_i/A_i is the charge-to-mass ratio of ion species i, and E_0 is a

free parameter with dimensions of energy. C_i is a normalization coefficient, proportional to the relative abundance of species i in the seed population. Neglecting transport and non-equilibrium effects, the power-law index γ is determined by the shock compression ratio. It is therefore explicitly taken to be the same for all species. The e-folding energy E_{0i}, on the other hand, reflects limits of the acceleration process, as imposed by escape from the shock region. Dependence on species and θ_{Bn} therefore resides in E_{0i}. The proportionality to $\mathrm{Q}_i/\mathrm{A}_i$ was first suggested by Ellison & Ramaty (1985) and has been found to give a consistent description of ion spectra in some SEP events (Tylka et al. 2000; 2001; 2006) and for ions accelerated locally by some traveling interplanetary shocks (Klecker et al. 2003). More generally, Tylka et al. (2000) found two SEP events in which E_{0i} scaled as $(\mathrm{Q}_i/\mathrm{A}_i)^{\delta}$, where $1 \leq \delta \lesssim 2$ and δ decreased with time. From consideration of proton-amplified wave growth at the shock, it can be shown that δ is generally not expected to deviate too much from unity for typical shock parameters. For simplicity, we take $\delta = 1$ in these calculations. See Section 10 for further discussion.

The dependence on θ_{Bn} in equation (2) is derived from equations (66) and (67) in Lee (2005a) based on the explicit θ_{Bn}-dependence in the expression for the proton rollover. This dependence includes the reduction of the ion escape rate from the shock by scattering parallel to the oblique magnetic field. Although this explicit θ_{Bn}-dependence hinges on the assumptions of the model presented by Lee (2005a) and omits implicit dependence on θ_{Bn} in his equation (66), equation (2) provides a reasonable representation of the reduced timescale for acceleration at quasi-perpendicular shocks. See Section 10 for further discussion of the form of equation (2).

Let $\xi = \cos\theta_{Bn}$. To represent the evolution of the shock and θ_{Bn} with time, we simply average equation (1) over the domain $\xi_{min} \leq \xi \leq \xi_{max}$, assuming that the evolution uniformly samples each incremental range of ξ between ξ_{min} and ξ_{max}. The flare component of the seed population is accessible to the shock at all ξ. However, to approximate the injection effects sketched in Figure 3, we introduce a heuristic weighting factor of ξ for the coronal component, so that its contribution becomes increasingly suppressed as the shock approaches perpendicular. Hence,

$$\overline{F}_{i,flare}(E) = C_{i,flare} E^{-\gamma} \int_{\xi_{min}}^{\xi_{max}} \exp(-E\xi^{2/(2\gamma-1)}/\check{E}_{0i,flare}) d\xi \Big/ \int_{\xi_{min}}^{\xi_{max}} d\xi \qquad (3)$$

$$\overline{F}_{i,coronal}(E) = C_{i,coronal} E^{-\gamma} \int_{\xi_{min}}^{\xi_{max}} \xi \exp(-E\xi^{2/(2\gamma-1)}/\check{E}_{0i,coronal}) d\xi \Big/ \int_{\xi_{min}}^{\xi_{max}} d\xi, \qquad (4)$$

where $\overline{F}_{i,flare}$ and $\overline{F}_{i,coronal}$ are the intensity of species i from the flare- and coronal-components[1] of the seed population, respectively, after averaging over θ_{Bn}. By a change of variable, these two equations can be expressed in a common form:

$$\overline{F}_i(E) = C_i E^{-\gamma} a_i^{-\rho} \left(\frac{2\gamma - 1}{2}\right) \int_{u_{i,min}}^{u_{i,max}} u^{\rho-1} \exp(-u) du / (\xi_{max} - \xi_{min}) \tag{5}$$

where $a_i \equiv E/\check{E}_{0i}$, $\rho = (2\gamma - 1)/2$ for the flare component and $\rho = 2\gamma - 1$ for the coronal component, $u_{i,min} = a_i \xi_{min}^{2/(2\gamma-1)}$ and correspondingly for $u_{i,max}$. These equations can be integrated numerically for arbitrary γ, ξ_{min}, and ξ_{max}. Averaging over the full range, $0 \leq u \leq a_i$, allows the following asympotic expansion:

$$\overline{F}_i(E) = C_i E^{-\gamma} \left(\frac{2\gamma - 1}{2}\right) \left\{\Gamma(\rho) a_i^{-\rho} - a_i^{-1} \exp(-a_i) \left[1 + (\rho - 1) a_i^{-1} + (\rho - 1)(\rho - 2) a_i^{-2} + \cdots\right]\right\}. \tag{6}$$

In the limit of sufficiently large energy $E >> \check{E}_{0i}$, so that the exponential suppresses the terms in square brackets, this expansion yields

$$\overline{F}_{i,flare} \sim C_{i,flare} (Q_{i,flare}/A_i)^{(2\gamma-1)/2} E^{(1-4\gamma)/2} \tag{7}$$

while

$$\overline{F}_{i,coronal} \sim C_{i,coronal} (Q_{i,coronal}/A_i)^{2\gamma-1} E^{1-3\gamma}. \tag{8}$$

---

[1]The reader may be tempted to think that the proper normalization in the denominator of equation (4) should be $\int_{\xi_{min}}^{\xi_{max}} \xi d\xi$, rather than $\int_{\xi_{min}}^{\xi_{max}} d\xi$. Our objective here is to average the particle production from a shock moving along a given trajectory, each element of which contributes to the fluence. The fluence is proportional to the average over all elements of the trajectory, which we perform as an average over ξ rather than an average over time. To see that our normalization factor of is indeed correct, consider the hypothetical case in which the shock is nearly perpendicular (that is, $0 \leq \xi \leq \epsilon$) along its whole trajectory, where ϵ is a small number. With the alternate normalization, the coronal contribution fails to vanish as ϵ approaches zero, in contradiction to the explicit intention of this formulation. A preliminary report on this model (Tylka 2005) used the incorrect coronal normalization. When averaging over a large range of ξ, the consequences of the incorrect normalization are minor, as can be seen by comparing Figure 3 of that paper with Figure 4 of this one.

Thus, the spectrum of the coronal component is steeper by an additional factor of $E^{-(2\gamma-1)/2}$, so that the flare component will increasingly dominate as energy increases, provided that $\gamma > 0.5$. (Actually, $\gamma > 1$ according to the theory of diffusive shock acceleration.) Moreover, by averaging over θ_{Bn}, we have also derived high-energy intensities (or fluences) that roughly scale as power-laws in Q_i/A_i, but with different power-law indices for the flare- and coronal components. This result will become important in Section 7.

At sufficiently low energies, equations (3) and (4) yield $\overline{F}_{i,flare}(E) = C_{i,flare}E^{-\gamma}$ and $\overline{F}_{i,corona}(E) = 0.5 \cdot C_{i,corona}E^{-\gamma}$, respectively, for integration over $0 \leq \xi \leq 1$. The calculation thus recovers the same spectral slope for all species. The low-energy limit also recovers the composition of the seed population, apart from the factor-of-two reduction in the relative size of the coronal component. This reduction arises from the relative suppression of the coronal component when $\xi < 1$. In reality, of course, spectral slope and composition at low energies can be particularly distorted by transport, co-rotation, and other shock evolution effects, as we will discuss later.

To perform calculations, we must specify the details of the seed populations. We use the average abundance ratios from Reames (1995b). For example, Reames (1995b) gives $< Fe/O > = 1.08\pm0.06$ for the flare component and $< Fe/O > = 0.134\pm0.007$ for the coronal component, so that $(Fe/O)_{flare}/(Fe/O)_{coronal} \sim 8$.

For each element, we must also sum over a distribution of ionic charge states. For the coronal component, we use theoretical distributions (Arnaud & Rothenflug 1985; Arnaud & Raymond 1992) corresponding to a temperature of T_{corona}=1.26 MK (i.e., $\log_{10}$T=6.1 in their tables). These distributions yield $<Q_{O,coronal}> = 6.0$ and $<Q_{Fe,coronal}> = 10.5$.

The appropriate charge-state distributions for flare particles is not well understood, particularly since their charge states (at least for Fe) increase with energy (Moebius et al. 2003; Klecker et al. 2005), probably due to stripping at or near the flare site. For the purposes of these calculations, except for Fe, we adopt theoretical charge-state distributions for flare ions corresponding to the temperature $T_{flare} = 4.0$ MK; Reames et al. (1994) found that temperatures of ∼3-5 MK yield mean Q/A values that roughly organize the abundance patterns in impulsive events (Reames & Ng 2004; Mason et al. 2004; see also Figure 12 below). This temperature corresponds to $<Q_{O,flare}> = 7.8$. For flare Fe, we use a Gaussian charge-state distribution with mean $< Q_{Fe,flare} > = 20$ (Luhn et al. 1987) and standard deviation $\sigma = 2.0$.

Finally, we quantify the relative sizes of the flare- and coronal components in the seed

population through a variable factor

$$R \equiv C_{oxygen,flare}/C_{oxygen,coronal}. \tag{9}$$

R reflects the relative strengths of the two components as they would be viewed by a parallel shock, where the issue of suppressed injection does not arise. Note that for $R = 0.05$, the different Fe/O ratios in the two components imply that $C_{Fe,flare}/C_{Fe,coronal} = 0.403$.

Thus, our calculations have three explicit free parameters, γ, E_0, and R. In principle, the temperatures T_{corona} and T_{flare} are also free parameters, which can be used to fine-tune the charge-state distributions. In practice, we will consider here only minor adjustments in T_{corona}, in the range of ∼1.2-1.6 MK, so as to match observed Fe charge states in individual events.

Most importantly, we must also reflect potential variability in the history of θ_{Bn}, as suggested by Figure 2. According to Jokipii (1987) and Webb et al. (1995), the advantages of quasi-perpendicular geometry become significant when θ_{Bn} exceeds 60 ° or 70 °, where the particles' rate of energy gain starts to rise sharply with increasing θ_{Bn}. We will therefore consider two cases in averaging over θ_{Bn}: either the full angular range $0 \leq \theta_{Bn} \leq 90\,^\circ$ (we will henceforth refer to this as the "quasi-perpendicular" case); or only $0 \leq \theta_{Bn} \leq 60\,^\circ$; (we will call this the "quasi-parallel" case).

Given the complexity we are trying to describe, this analytical formulation may appear to be in danger of being too simple. Nevertheless, as we shall see, it is remarkably successful in reproducing key features of the data. But we also note in passing that the formulation admits other sources of variability that we have chosen not to exploit. In all of our calculations, we use only the nominal composition for the flare- and coronal components of the seed population, as given by Reames (1995b); we make no attempt to consider intrinsic variability in the elemental composition of the seed populations, apart from the relative normalization of the two components. In addition, we have chosen to suppress the coronal component at quasi-perpendicular shocks with a simple factor of $\xi = \cos\theta_{Bn}$. But more generally ξ^α, where $\alpha > 0$, could also be invoked to reflect details in the injection process. Different values of α can change the relative spectral index of oxygen and iron at high energies (see Figure 4c below) and hence the slope with which Fe/O grows with energy. Moreover, the integrals in equations (3) and (4) could also contain a function of ξ to account for the relative amount of time that the shock has different values of ξ; our quasi-perpendicular and quasi-parallel cases are simply two particular choices for that function.

4. Model Calculations

For purposes of illustration, let us consider γ=1.5, corresponding to a compression ratio of 2.5. Typical coronal magnetic fields (Gopalswamy et al. 2001; Mann et al. 2003) and plasma densities (Mann et al. 1999) yield γ values (Ellison & Ramaty 1985) in the range of ∼1.3 to ∼1.7 for a shock speed of 1750 km/s at altitudes of ∼2-10 R_S from Sun center. This speed is close to the average CME speed (1708 km/s), as measured by *SOHO* (Yashiro et al. 2004) at roughly these same coronal altitudes, among the large SEP events listed in Tylka et al. (2005). SEP timing studies (Bieber et al. 2004; Cliver 2006; Kahler et al. 2003; Mewaldt et al. 2003; Sáiz et al. 2005, Tylka et al. 2003) indicate that high-energy SEPs are produced when CMEs are at these altitudes. For γ=1.5, the integrals in equations (3) and (4) can be expressed in closed form. Numerically-integrated results for other γ values are qualitatively similar.

Figure 4 shows two calculations, both with $\gamma = 1.5$, $E_0 = 3.0$ MeV/nucleon, and $R = 0.05$. The two calculations differ only in the averaging range for θ_{Bn}, either quasi-perpendicular or quasi-parallel, as explained above. Except for the Fe/O below ∼1 MeV/nucleon, which we will address later, the energy-dependence in these results is qualitatively similar to that in the two extreme events discussed in Tylka et al. (2006). (One of these extreme events, 2002 April 21, is better described using R=0, as shown in Section 7. But our intent here is to illustrate the consequences of changing only one aspect of the calculation, the θ_{Bn} range.)

In the calculations of Figure 4, a quasi-perpendicular shock produces Fe/O that rises with energy and a roughly double-power-law oxygen spectrum. Omitting the quasi-perpendicular range of shock angles produces Fe/O falling with energy and an oxygen spectrum that rolls over roughly exponentially.

Figure 4c offers a closer look at the iron and oxygen spectra in the quasi-perpendicular case at energies of 5-100 MeV/nucleon, where the rise in Fe/O with energy is often observed. The model calculations for both spectra are roughly power-laws over this restricted range. However, the apparent power-law indices are different for the two species, with iron harder than oxygen, just as we see in the data (Tylka & Dietrich 1999; Tylka et al. 2002, 2006). Moreover, the magnitude of the spectral difference is also comparable to what we find in the data. In these particular calculations, the spectral indices differ by 0.40, matching the difference of 0.36 ± 0.03 found in the 2001 April 15 GLE (Tylka et al. 2002; see also Lehtinen et al. 2005). Different power-laws for different species has been touted as an ostensible challenge for explaining these data in terms of shocks. But this calculation shows that species-dependence can arise naturally in the context of shock acceleration, even though the calculation explicitly started with the same power-law index for all species.

A closer examination of the results in Figure 4c shows that the calculated iron spectrum is approximated by a single power-law to within deviations of only ∼2%. For the oxygen spectrum, the deviations from a single power-law are larger, approaching ∼15% at the ends of the energy range. In practice, such deviations are difficult to detect with current instrumentation, especially given systematic differences among the several instruments needed to cover this whole range. Also, these simplified calculations do not include other factors that would tend to cause both O and Fe spectra to bend downwards at high energies. One such factor would be non-zero $K_\perp/K_\parallel$, where $K_\perp$ and $K_\parallel$ are diffusion coefficients perpendicular and parallel to the mean magnetic field, respectively.

Figure 5a shows additional model calculations, in which we have varied R, the relative strength of the flare- and coronal components in the seed population. Note that the e-folding energy E_0 is the only energy scale in the calculations; the curves can therefore be shifted horizontally by changing its value. We have already shown (Tylka et al. 2000, 2002, 2006) examples of events in which Fe/O rises to nearly the impulsive value or falls precipitously with energy. We will discuss in Section 6 an event in which Fe/O starts to decline but then "bottoms out" and recovers, similar to the curves in the middle of Figure 5a. The 1998 May 6 GLE has enhanced Fe/O at ∼4 times the coronal value but with little energy dependence (Tylka et al. 2005). Thus, the calculations in Figure 5a display the same "zoo" of behavior as found in the data.

Before we examine the implications of these calculations, it is worthwhile to ask how our assumptions have contributed to these results. Could the averaging over θ_{Bn}, combined with the different composition and charge states of the flare- and coronal seed particles, be adequate in themselves to account for the event-to-event variability in the data? In particular, is the additional factor of ξ in the integrand of equation (4), which serves to suppress the coronal contribution at quasi-perpendicular shocks, really necessary? What sort of results would we obtain if we were to use equation (3) for *both* flare- and coronal components?

To address these questions, Figure 5b shows calculations with the same parameters as in Figure 5a but using equation (3) for both components, thereby abandoning the coronal suppression factor. The characteristics of these calculations are easily understood: at low energies, the Fe/O ratio is a straightforward reflection of the input mixture of flare- and coronal seed particles. At high energies, both components have simply been reduced in the quasi-perpendicular calculations by the appropriate value of Q_i/A_i, as demanded by equation (7) for $\gamma = 1.5$. Unlike the results in Figure 5a, the calculations in Figure 5b are *not* representative of the energy-dependent-Fe/O morphologies seen in the data. Thus, although the formulation in equations (3) and (4) is certainly a crude proxy for a complicated

physical process, the differences in injection likelihoods for coronal and flare seed particles that are thereby represented are clearly essential for the success of our model. (Further discussion refers exclusively to Figure 5a.)

5. Average value of enhanced Fe/O at high energies

The upper right of Figure 5a shows a surprising result: no matter how large the flare component in the seed population, when the ions are processed through a shock, the high-energy Fe/O never recovers the input flare value. The origin of this result is easy to see: at sufficiently high energies, the coronal component becomes negligible in equation (8). The linear Q/A-dependence of the flare component for $\gamma = 1.5$ in equation (7) therefore leads to

$$\begin{aligned} Fe/O &= (C_{Fe,flare}/C_{O,flare})(<Q_{Fe,flare}>/56)/(<Q_{O,flare}>/16) \\ &= 1.08 \cdot (20/56)/(7.8/16) \\ &= 0.79, \end{aligned} \tag{10}$$

which is 5.9 times the nominal coronal value.

But do we see this behavior in the data? Starting with the event list in Tylka et al. (2005), we used data from the Solar Isotope Spectrometer (SIS; Stone et al. 1998) on *ACE* to determine the Fe/O ratio for each event in several energy bins. In each energy bin, we kept only those events in which Fe/O exceeded three times the nominal coronal value. Histograms for three of these energy bins are shown in Figure 6. In each case, the Fe/O values cluster close to ∼5 times the coronal value and are well below the average found in impulsive events.[2]

Figure 7 shows the weighted mean from each bin plotted versus energy. The figure includes both data from *ACE*/SIS in 1997-2003 and results from an identical analysis of observations from the University of Chicago's Cosmic Ray Nuclei Experiment (CRNE; Garcia Munoz et al. 1975) on *IMP-8* from 1974-2001. The dashed black lines in Figure 7 indicate the expected asymptotic value from equation (10), given two different reasonable values of $< Q_{Fe} >$. These asymptotes were evaluated with $\gamma = 1.5$. Larger γ (or smaller γ, which would be rare) will move the asymptotes downward (or upward) but do not change

[2]Recent re-analysis of SIS heavy-ion measurements shows that the Fe/O (and Fe/C) values first reported by Cohen et al. (1999a, b) were systematically high (C. Cohen, private communication). The results of the re-analysis agree with our values.

the qualitative result. The observed average values at all energies are below or near the calculated asymptotes; in no case do they attain the flare average, not even at the highest measureable energies. On the contrary, there is a hint in Figure 7 that Fe/O, at least on average, begins to decline above ∼100 MeV/nucleon. This behavior might reflect a rollover in the spectra from quasi-perpendicular shocks due to other factors, such as finite shock-size or non-zero $K_\perp/K_\parallel$, which are not taken into account in our calculations.

It must be remembered that the Fe/O ratio varies among impulsive events (see Figure 6, Reames et al. 1994); presumably the charge states do so as well. These variations will be reflected at some level in the seed population formed by flare ions. Thus, this analysis emphatically does not preclude *individual* gradual events in which Fe/O exceeds ∼6 times the coronal value. However, given what we know about the *average* characteristics of flare ions, we can make a prediction about the *average* results when those ions are further accelerated by a shock. Figure 7 shows that this expectation is consistent with a heretofore-unexplained feature of thirty years of SEP observations. By the same token, the results in Figure 7 are an important quantitative challenge for scenarios that attribute the high-energy Fe/O enhancements to a *direct* flare component, unaided by processing through a shock (e.g., Cane et al. 2003).

6. The Shock Event of 2001 November 6

As shown in Figure 4, highly-supressed Fe/O occurs when the quasi-perpendicular phase is absent from the shock's evolution. But when the quasi-perpendicular phase is present, Figure 5a offers another surprising prediction: as shown by the R=0 curve in the middle of the plot, the high-energy Fe/O will "bottom out". The origin of this result is seen in equation (8), evaluated at $\gamma = 1.5$. When the flare component is absent and energy is sufficiently high, the minimum value of Fe/O is given by

$$\begin{aligned} Fe/O &= (C_{Fe,coronal}/C_{O,coronal})(<Q_{Fe,coronal}>/56)^2/(<Q_{O,coronal}>/16)^2 \\ &= 0.134 \cdot (10.5/56)^2/(6.0/16)^2 \\ &= 0.034, \end{aligned} \tag{11}$$

which is 0.25 times the nominal coronal value.

Figure 8 shows an event that may illustrate these very circumstances. A strong shock arrived at Earth on 2001 November 6. The shock was associated with the fast CME that

departed 33 hours earlier from a source region at W18° with an initial speed[3] of 1810 km/s. This shock produced the highest intensity of >10 MeV protons seen at Earth so far in Cycle 23.[4] *GOES* also reported increases in protons above ∼500 MeV in association with the shock's arrival. As seen in the top panel of Figure 8, the intensities of ions above ∼30 MeV/nucleon were higher when the shock arrived than they were at the event's onset. This extraordinary shock was quasi-perpendicular near Earth, with $\theta_{Bn} = 82 \pm 3\,^\circ$, as determined from a multi-pairing analysis of magnetic coplanarity, using 16-s data from the *ACE*/MAG experiment (Q. Hu, private communication). Thus, in this event we are certain that the shock's evolution contained at least one quasi-perpendicular phase, simply because that phase occurred near Earth. In addition, the *Solar, Anomalous, and Magnetospheric Particle Explorer (SAMPEX)* reported charge states above ∼25 MeV/nucleon in this event as $<Q_{Fe}>= 12 \pm 1$ and $<Q_O>= 6.6 \pm 0.3$ (Labrador et al. 2003). These charge states are consistent with little or no flare particles in the seed population.

The bottom panel of Figure 8 shows the event-integrated Fe/O versus energy for this event. As energy increases, Fe/O begins to decline, reaches a minimum of about ∼0.25 times coronal, and then rebounds. Qualitatively, this behavior has a shape similar to the quasi-perpendicular case in Figure 5a, in which R=0.0005, corresponding to an almost complete absence of flare particles in the seed population. Of course, one cannot draw general conclusions from a single event. But nevertheless, given the measurements of θ_{Bn} and the charge states, it appears that this event behaved just as we would expect.

The event of 2001 September 24 (Figure 9) offers a tantalizing comparison. This CME was similar to that of 2001 November 4; it launched from near the center of the solar disk, from a source region at E23° with an initial speed of 2402 km/s and a Sun-Earth transit time of 34.5 hours. The measured *SAMPEX* charge states above ∼25 MeV/nucleon (discussed below, in Figure 14) were $< Q_{Fe} > = 10.2 \pm 2.0$ and $< Q_O > = 6.3 \pm 0.4$ (Labrador et al. 2003). To within measurement uncertainties, these values are the same as those in the November event. But in contrast to the November event, Fe/O in this event drops precipitously with energy, falling to just ∼ 3% of coronal at ∼60 MeV/nucleon. Our calculations ascribe this sort of behavior to an event in which the quasi-perpendicular phase is absent from the θ_{Bn} evolution. Of course, we do not know for certain that this is what actually happened in this event. But other features of the event are consistent with this suggestion. For example, compared to to the November event (Figure 8), the higher-energy time-intensity profiles here have a much slower rise and a more extended and rounded

[3]CME speeds were provided by *http://cdaw.gsfc.nasa.gov/CME_list/* (Yashiro et al. 2004).

[4]See *http://umbra.nascom.nasa.gov/SEP/seps.html*.

shape, without the "spike" near the time of shock arrival. These characteristics are generally associated with quasi-parallel shocks (Tsurutani & Lin 1985), at least at lower energies. The measured shock-normal angle in this event at the time of arrival at *ACE* was $\theta_{Bn} = 66 \pm 18\,^\circ$ (Q. Hu, private communication), only poorly determined but not inconsistent with quasi-parallel. Thus, the shock-geometry hypothesis provides a plausible quantitative explanation for the dramatically different behavior in high-energy Fe/O in these two events.

(It is perhaps worth noting that these two events may also have differed in their shock-geometry characteristics near the Sun. As discussed in Section 9 below, because of their rapid acceleration time scales, quasi-perpendicular shocks are also attractive candidates for the cause of GLEs. The launch of the 2001 November 4 event produced a GLE; 2001 September 24 did not.)

7. Breneman & Stone Q/A Fractionation

Thus far we have focused on the Fe/O ratio. But other relative abundances also vary from event to event. Figure 10a shows results from *ACE*/SIS on the relative abundances of C, N, O, Ne, Mg, Si, S, Ca, and Fe at 12-60 MeV/nucleon for the events of 2001 April 15 (in red) and 2002 April 21 (in blue). These data illustrate one of the fundamental facts of SEP phenomenology, first discovered by Breneman & Stone (1985): when the relative abundances of heavy-ions are normalized to the mean values from many SEP events, the results are organized roughly as a power-law in Q/A. (See Reames 1998 for discussion of the approximate nature of the power-law ordering.) Moreover, the slopes of these power-laws vary from event to event. In some cases, Fe/O is suppressed relative to the mean, and the power-law has a positive slope. In other events, Fe/O is enhanced relative to the mean and the power-law has a negative slope. In making these power-laws, we rarely have actual charge-state values for the ions. Following Breneman & Stone, Figure 10 therefore employs nominal mean charge-state values, based on a survey of large gradual SEP events by Luhn et al. (1984). These nominal mean charge-states are intermediate between those we have used in our calculations for the coronal and flare components of the seed population.

Figure 10b shows results from our calculations. In both of these events, we chose values of E_0, γ, and R to roughly match the oxygen and iron spectra above a few MeV/nucleon. (See Figure 11 for details.) For one event in Figure 10b (in blue) R=0, so that no flare ions were in the seed population; for the other (in red) R=0.05. The two calculations also differed in the evolution of the shock geometry: for the event in red, we averaged over the full angular range, $0 \le \theta_{Bn} \le 90\,^\circ$; for the event in blue, only over $0 \le \theta_{Bn} \le 60\,^\circ$. The relative abundances and charge states of the seed populations were as specified in Section

3, except that T_{corona} in the 2002 April 21 event was slightly increased to 1.58 MK (that is, $\log_{10}$T=6.2) so as to better match the charge states reported for this event by Tylka et al. (2006).

We integrated the calculated spectra over 12-60 MeV/nucleon, the same energy range used in the data. The resulting elemental ratios were normalized to the gradual SEP-averages given by Reames (1995b); these are the same values that serve as nominal coronal composition in our calculations. Finally, the results were plotted against the same nominal Q/A values used by Breneman & Stone. (If the model results are plotted against the "actual" Q/A values – as derived from the model calculations – the blue line would be flatter and the red line would be steeper.)

For both the data and the model, we fitted the abundances to a power-law in Q/A. These fits are also shown in Figure 10. Although there are some points of disagreement, the data and model calculations are strikingly similar, as evidenced by the values of the fit parameters and the correlation coefficients. Although we show here only two events, varying the model parameters makes it possible to simulate events with other slopes.

The basis for this approximate power-law behavior was already seen in equations (7) and (8). For the coronal component with $\gamma = 1.5$, we expect the fluences to scale as $C_{i,coronal} \cdot (Q_i/A_i)^{+2}$. The modeled abundances follow a slightly steeper power-law (with a slope of 2.18 ± 0.12) almost entirely because we are plotting against nominal Q values that are systematically larger than the "actual" Q values of the coronal seed population.

On the other hand, for the flare component, equation (7) says that the fluences scale as $C_{i,flare} \cdot (Q_i/A_i)^{+1}$. But, as shown in Figure 12, except for protons and ^{3}He, the flare component's intrinsic composition relative to the corona is also roughly organized as a power-law,

$$C_{i,flare} \sim C_{i,coronal} \cdot (Q_{i,flare}/A_i)^{-3.8\pm0.3} \tag{12}$$

where $Q_{i,flare}$ is the mean charge corresponding to a 4.0 MK temperature. Combining this result with equation (7) therefore changes the slope of the flare-component from +1 to ~ -2.8. The modeled slope (-1.96± 0.36) is somewhat flatter, primarily because the nominal Q values used in Figure 10 are too small. Other factors also contribute to the flattening of the slope, as well as departures from perfect power-law behavior. These factors include the contribution of the coronal component, the scattering of average impulsive abundances around the power-law (Figure 12), and the details of the species-dependent energy spectra arising from equations (3) and (4).

Thus, we have explained why relative abundances in gradual events are roughly ordered as power-laws in Q/A, and why those power-laws can show either positive or negative slopes. At the same time, the calculations also account for differences in spectral shapes (Figure 11). To our knowledge, these calculations are the first quantitative explanation of the Breneman & Stone fractionation effect.

Finally, we note in passing that the effects described here are also likely to be relevant to event-to-event variation in isotopic fractionation among $Z > 2$ ions in gradual SEP events (Leske et al. 2003).

8. Other Compositional Signatures

The preferential acceleration of flare seed particles to high energies by quasi-perpendicular shocks should also be reflected in other compositional signatures. Figure 13 shows the measured ^{3}He/^{4}He ratio as a function of energy in the 2001 April 15 GLE, the same event shown in Figures 10 and 11 and in which Fe/O increases with energy. The curve is calculated with the same model parameters as used previously for this event. For the coronal component of the seed particles, we have set ^{3}He/^{4}He = 0.04%, the average value found in the solar wind (Gloeckler & Geiss 1998). For the flare component of the seed population, we have taken ^{3}He/^{4}He = 5.0%. This value was chosen to roughly match the high-energy measurements in Figure 13. However, it may also be relevant that the same active region produced one of the largest impulsive events of Cycle 23 just ∼18 hours prior to this GLE. In that impulsive event, *ACE* measured ^{3}He/^{4}He = 6.5 ± 1.2% at 0.5-2.0 MeV/nucleon (Tylka et al. 2002). The rise in ^{3}He/^{4}He with energy in Figure 13 means, of course, that ^{3}He has a harder spectrum than ^{4}He. This behavior has been previously reported at energies above ∼50 MeV/nucleon (Chen, Guzik, & Wefel 1995; see also Torsti et al. 2002).

Figure 14 compares model calculations for $<Q_{Fe}>$ and $<Q_O>$ versus energy to *SAMPEX* measurements for two events. The model parameters for the 2001 April 15 calculation are the same as before. The parameters for the 2001 September 24 event were the same as in the 2002 April 21 event (Figures 10 and 11), except that we used T_{corona} = 1.26 MK, so as to better match the observed Fe charge state above ∼25 MeV/nucleon. (We show 2001 September 24 charge states here because only limited *SAMPEX* measurements are available for the 2002 April 21 event. See Tylka et al. 2006 for further discussion.)

In both Figure 13 and Figure 14, the calculations show general trends that are similar to the data. But the calculations do most poorly in matching the observations below ∼1 MeV/nucleon. The observed ^{3}He/^{4}He and $<Q_{Fe}>$ lie below the curves, indicating that the

flare seed particles are over-represented at low energies in our calculations. This discrepancy is not surprising: whereas high-energy particles tend to be produced mostly near the Sun, these low-energy particles are produced more or less continuously as the shock moves outward. For most of that journey, the shock tends to be quasi-parallel, so that flare-seeds have lost their preference in the injection process. Our simple averaging over θ_{Bn} may be adequate for particle production near the Sun. But it almost surely fails to give adequate weight to the later history of the shock. A proper accounting of this production history will naturally dilute the contribution from flare seed particles at low energies.

Finally, as previously discussed, impulsive events also show ∼100-1000-fold enhancements in ultraheavy ions with atomic number Z > 34 (Reames 2000; Reames & Ng 2004; Mason et al. 2004). When these ions are further accelerated by a quasi-perpendicular shock, on average we would expect the flare-enhanced values to be reduced by a factor of Q/A, just as in equation (10). The appropriate Q/A values could be as low as ∼0.1 (Post et al. 1977). But if the flare process subjects ultraheavy ions to the same degree of additional stripping that flare Fe ions apparently experience, the appropriate Q/A values for the ultraheavy ions could be as large as ∼0.3. Thus, in either case, we would expect average ultraheavy enhancements at high energies in Fe-rich gradual events to be substantially smaller than the average ultraheavy enhancements in impulsive events. At present, we have no experimental information on the charge states of ultraheavy ions or their relative abundances above ∼10 MeV/nucleon in Fe-rich gradual events.

9. Other Implications of the Shock-Geometry Hypothesis

As discussed in Tylka et al. (2005), the shock-geometry hypothesis may also help to resolve other puzzles about the high-energy SEP data:

(1) Event size, as measured by total proton fluence, is potentially affected by many factors. If the seed population comprised two components (coronal plus flare), one would generally expect a larger fluence than if the seed population comprised just one component (coronal). By this reasoning, events that are Fe-rich at higher energies should be *larger*, at least on average. But this is exactly the opposite of what we see in the data: events with enhanced high-energy Fe/O tend to have *smaller* proton fluences above 30 MeV. (See Tylka et al. 2005, Figures 6 and 9.) Some additional factor must therefore be coming into play. Shock geometry is a plausible candidate for this additional factor: the higher injection threshold at quasi-perpendicular shocks not only favors flare suprathermals but also discriminates against the large, slower part of the coronal component. (See Figure 3.)

(2) The evolutionary history of θ_{Bn} near the Sun should also be reflected in the shapes of the SEP time-intensity profiles at high energies. The acceleration rate at a quasi-perpendicular shock in the corona can be fast, with some estimates indicating that particles can attain ∼GeV energies in just a few tens of seconds. (See, for example, Figure 1 above and Giacalone 2005a.) In such cases, the rise to maximum intensity can be quite sharp. On the other hand, for a shock that is quasi-parallel near the Sun, high-energies cannot be attained until a spectrum of Alfvén waves – sufficient to continuously scatter particles back and forth across the shock even as their energies increase – has been grown from the pre-exisiting background. Compared to the acceleration rate at the quasi-perpendicular shock, this wave-growth process is generally expected to be slow; the high-energy time-intensity profiles will therefore have a more gradual onset. (See, for example, Figure 3 of Tylka et al. 2006.)

In addition, the production rate of high-energy particles will fall precipitously when θ_{Bn} decreases from quasi-perpendicular values; the high-energy time profiles from quasi-perpendicular shocks will therefore naturally have a more "impulsive" appearance. But once the necessary wave intensities have been established at a quasi-parallel shock, the production rate will decay more slowly, probably governed more by the fall-off in the ambient magnetic field strength rather than by further changes in θ_{Bn}. Of course, all of these scenarios must be evaluated in the context of a full-fledged transport model. Nevertheless, these considerations may explain why events that are Fe-rich at high energies also tend to have shorter durations at those energies. (See Figures 11 and 12 in Tylka et al. 2005.)

(3) Because of their rapid acceleration time-scales, quasi-perpendicular shocks are also particularly good at making GeV particles. We would therefore generally expect GLEs to be Fe-rich at high energies. In fact, ∼85% of GLEs in 1973-2005 were Fe-rich at energies of ∼40 MeV/nucleon or higher (Dietrich & Lopate 1999; Tylka et al. 2005). By comparison, only ∼40% of large, non-GLE events are Fe-rich at high energies. Of course, flare ions need not be present in the seed population for every GLE. This may have been the case in the historic 2005 January 20 GLE, which occurred very late in the Solar Cycle, when both the overall rate of flare activity[5] and the potential pool of flare seed particles, as reflected by *ACE* measurements of ^{3}He in the interplanetary medium (M. Wiedenbeck, private communication), had declined. In this GLE, at no energy is the event-integrated Fe/O enhanced by more than a factor of ∼two over the nominal coronal value, and the measured charge states

[5]From *Solar Geophysical Data Online* at ftp://ftp.ngdc.noaa.gov/STP/SOLAR_DATA/SOLAR_FLARES/HALPHA_FLARES/PDF_Tables/Number_of_Solar_Flares.pdf.

above ∼20 MeV/nucleon for C, O, Ne, Mg, Si, and Fe are all consistent with a common temperature of ∼1.6 MK (Labrador et al. 2005).

(4) Finally, the difference in the spectral rollover energy will cause a quasi-perpendicular shock to have a harder spectrum at high energies than a quasi-parallel shock with the same speed (see Figure 1). This tendency may help to explain why events that are Fe-rich at high energies are observable over a wider range of source longitudes (see Figure 13 in Tylka et al. 2005) and at smaller CME speeds than other events (Figure 19 in Tylka et al. 2005). But this issue must be addressed through detailed modeling, in order to take into account the contravening effect of the size of the accessible seed population.

10. Caveats, Limitations, and Summary

The shock-geometry hypothesis potentially addresses a wide range of SEP phenomenology, including variability in spectral shapes, energy-dependent composition and charge states, Breneman & Stone fractionation, average Fe enhancements at high energies, event size, Fe-richness in GLEs, and perhaps even the shapes of high-energy time profiles and SEP event distributions in source longitude and CME speed. Some of these observations have not been explained before. For others, it is certainly possible to craft alternative explanations. But a strength of the shock-geometry hypothesis is that it potentially addresses all of these features of the data, as well as the correlations among them. Moreover, all of these facets of high-energy variability are accounted for within the context of the parameter variation that is inherent in shock acceleration, rather than appealing to multiple acceleration mechanisms. However, the approximations and assumptions behind our calculations must kept in mind.

First of all, we should emphasize that the form of F_i in equations (1) and (2) has not been derived from first principles. In particular, the exponential dependence on energy and the proportionality $E_{0i} \propto Q_i/A_i$ follow most directly from observations (Ellison & Ramaty 1985; Klecker et al. 2003; Tylka et al. 2000, 2001, 2006). The dependence of E_{0i} on $\sec\theta_{Bn}$ employed here arises from the explicit dependence in the primary model of Lee (2005a) [his equations (66) and (67)]. However, E_{0i} surely also has implicit dependence on θ_{Bn}, through the speeds of the injected protons and the proton injection rate, which are unknown and controversial. Moreover, the primary model of Lee (2005a) does *not* yield the exponential form in equations (1) and (2). The actual dependence of the high-energy rollover on E, Q_i/A_i, and θ_{Bn} follows from the dependence of the upstream wave intensity $I(k)$ on wavenumber k, distance from the shock, and θ_{Bn}, and from the dependence of the spatial diffusion tensor on $I(k)$. These quantities are not well known, particularly the form of $K_\perp$.

On the other hand, the secondary model presented by Lee (2005a) [his equations (92), (93), and (98)], based on the reasonable assumptions that $I(k)$ is dominated by a proton-excited component proportional to k^{-1} and that $K_\perp/K_\parallel$ is small, actually *does* predict an exponential rollover in energy with $E_{0i} \propto (Q_i/A_i)(\sec\theta_{Bn})^\lambda$, where $0 < \lambda < 2$. Although the dependence $I(k) \propto k^{-1}$ is not derivable with rigor, Lee (2005b) has shown that $I(k)$ consists of a double power-law, with $I(k) \propto k^{-2}$ at high k and $I(k) \propto k^{2(\gamma-2)}$ at low k. For $\gamma = 1.5$ (the value we used in our calculations), $I(k) \propto k^{-1}$ at low k, as required. More generally, this double power-law for $I(k)$ could yield a rollover in energy close to that produced by $I(k) \propto k^{-1}$. Thus, although the proper form of F_i poses a number of theoretical challenges, equations (1) and (2) are nevertheless a reasonable and simple starting point. We have shown that even this simple form leads to unanticipated and important consequences, which we hope will spur progress on more accurate representations of F_i.

Our calculations make no attempt to account carefully for the actual forms of the seed-particle velocity distributions or the details of the injection and acceleration processes. These processes would presumably impact the choice of weighting factors in equations (3) and (4), here taken to be 1 and ξ, respectively. As we have noted in several places, our calculations also ignore the impact of non-zero $K_\perp/K_\parallel$, which would serve to remove the singularity by which the e-folding energy in equation (2) becomes infinite at $\theta_{Bn} = 90\,^\circ$. Our calculations also neglect transport effects, under the assumption that those distortions are likely to be less significant at higher energies. In spite of these omissions, these calculations comprise a valuable first step: they capture the essential features of the shock-geometry hypothesis in a simplified way that is well-motivated by both theory and observations. These heuristic calculations are therefore precisely the sort of demonstration one would want to see before embarking upon the arduous tasks needed for a rigorous treatment.

A crucial element in our formulation is the notion that particles must have a higher initial speed in order to be efficiently accelerated at quasi-perpendicular shocks. Most theoretical investigations (Forman & Webb 1985; Jokipii 1987; Webb et al. 1995; Zank et al. 2004) have favored this idea. The notion of θ_{Bn}-dependent efficiency has also been invoked to explain features of energetic particle observations in other contexts, ranging from Earth's bow shock (Meziane et al. 2002) to the heliospheric termination shock (McComas & Schwadron 2006). But Giacalone (2005a,b) has recently challenged this consensus. Using numerical simulations he found that, at least under some scattering conditions, the injection threshold is only weakly dependent on θ_{Bn}. If this result is correct, spectral variability alone would still argue that differences in θ_{Bn} are important for SEP production near the Sun. But if the injection threshold does not vary with θ_{Bn}, we lose the link between spectral shape and high energy Fe/O, which is so clearly demanded by the data (see Figure 9 in Tylka et al. 2005). We also lose our explanation for Fe-richness in GLEs and the tendency for Fe-rich events to

have smaller fluences. Further theoretical clarification is therefore needed in this matter. Of course, we do not know the scattering conditions in regions of the corona where high-energy SEPs are generally produced. It may therefore be worthwhile to turn the problem around and to ask how SEP characteristics can be used to infer constraints on coronal conditions.

It is also important to keep in mind issues that are left unaddressed by these calculations. For example, the e-folding energy-scale, E_0, is a completely free parameter. But in reality, it should reflect a number of factors, such as finite shock-size and near-shock scattering conditions. The latter are expected to be largely determined by self-generated Alfvén waves, at least in the case of quasi-parallel shocks. Our calculations give no insight into that issue or other conditions that may govern event-to-event variation in E_0. For reasons of both practical application and proper treatment of non-linear wave growth (Ng, Reames, & Tylka 2003; Lee 2005a), a comprehensive SEP model must also deal in absolute intensities; these calculations do not do that.

A particular challenge for future work is to verify that the apparent successes of the shock-geometry hypothesis survive when it is implemented within a realistic model of a CME-driven shock. For example, we have focused on only the evolution in θ_{Bn}. But other key parameters, such as the compression ratio, seed particle densities, and ambient plasma conditions, also evolve; these factors must also be taken into account. When these calculations are further tied to a careful treatment of particle transport (such as Ng et al. 2003), it should also be possible to evaluate the hypothesis by comparison with time-dependent spectra and abundance ratios (e.g., Tylka et al. 2006), rather than just the event-integrated quantities we have used here.

The behavior below ∼1 MeV/nucleon provides an example of where more realistic treatments are probably essential for remedying the shortcomings of these calculations. As we have already discussed, we fail to match measured ^{3}He/^{4}He and $< Q_{Fe} >$ at these energies, probably because our calculations give inadequate weight to particle production at later stages in the shock's transit from the Sun. The model spectra in Figures 11 also diverge from the data at energies below ∼1 MeV/nucleon. In both cases, the data tend to lie below the calculated spectra, with oxygen farther below than iron. As a result, the Fe/O ratio at these energies is higher in the data than in the calculations. (Compare Figure 1 from Tylka et al. 2005 with Figure 4a in this paper.) Comprehensive surveys from *SAMPEX* and *ACE* on gradual-event charge states below ∼1 MeV/nucleon have not yet been published. But in the data we have seen, Fe has a relatively low charge state, typically ∼9-12. As a result, Fe likely scatters less than O at the same energy. This difference in scattering rate — combined with comparatively long particle travel times from the Sun, the sweep of the observer's connection point across the shock front, and co-rotation — can lead to significant distortions

in the Fe/O ratio at low energies, even after integrating over an event's entire duration. Of course, all of these concerns become less acute as we move toward higher energies, where the particle speeds are faster, the scattering mean free paths are longer, and the particle production is more likely to have shorter duration and to be concentrated near the Sun.

In summary, additional work is needed to test the shock-geometry hypothesis and to put it on a firmer theoretical and observational basis. As discussed in more detail in Tylka et al. (2005), critical questions also remain: are there adequate numbers of flare suprathermals in the corona to provide the seeds for the observed high-energy fluences in Fe-rich events? Do scattering conditions in the corona allow for a higher injection-threshold at quasi-perpendicular shocks? Can we find direct imaging or spectroscopic confirmation for our inferences about coronal shock geometry in individual events? In spite of these questions, the calculations presented here and their close correspondence with a wide range of SEP observations leave us optimistic that the complexity of high-energy variability can indeed be encompassed in terms of shock physics for most, if not all, large SEP events.

Finally, we also reaffirm the fundamental correctness of the two-class paradigm enunciated by Reames and others. There are indeed two distinct mechanisms for accelerating solar particles, one associated with flares and the other with shocks. Whereas the flare acceleration mechanism introduces strong compositional distortions by means that are still only vaguely understood, shock acceleration reflects the composition of the seed population in ways that are complicated but nevertheless becoming clearer. The complementary roles of flares and shocks in large, gradual SEP events is more subtle than we had realized, with the former being an important source of seed particles for the latter, especially at high energies, where the production often occurs at quasi-perpendicular regions of the shock. In some sense, we should have forseen this connection. After all, the distinctive advantages of quasi-perpendicular shocks (Jokipii 1982; 1987; Sarris & Krimigis 1985), their likely existence on the flanks of CMEs (Steinolfson 1984), and the injection-threshold bias (Forman & Webb 1985; Jokipii 1987) have been known for nearly two decades. We have also long known that impulsive events are sufficiently frequent at solar maximum, that their particles persist as a potential seed population for shocks even when no flare is going on (Richardson et al. 1990). But we needed the precise and challenging observations provided by the new spacecraft of Cycle 23 to spur this synthesis of what we already knew.

It is a pleasure to acknowledge our many generous colleagues who provided data and/or informative and helpful discussions in the course of this work. We thank E.W. Cliver, C.M.S. Cohen, W.F. Dietrich, J. Giacalone, Q. Hu, J.R. Jokipii, A.W. Labrador, R.A. Leske, G. Li, C.G. Maclennan, G.M. Mason, J.E. Mazur, R.A. Mewaldt, R.J. Murphy, C.K. Ng, D.V. Reames, G.H. Share, M.E. Wiedenbeck, and G.P. Zank. We also thank the anonymous

reviewer for helpful suggestions that improved the paper, including the asymptotic expansion given in equation (6). We gratefully acknowledge data provided by the *ACE* Science Center, NSSDC, NOAA, and the *SOHO*/LASCO CME catalogue, which is generated and maintained by NASA and The Catholic University of America in cooperation with the Naval Research Laboratory. This work has been supported in part by NASA's Living with a Star Targeted Research and Technology Program under DPR NNH05AB581. AJT was also supported by the Office of Naval Research and NASA DPR S13791G. MAL was also supported by NSF Grant ATM-0091527, NASA Grant NNG05GL40G, and DoD MURI grants to the University of Michigan and the University of California at Berkeley.

Facilities: ACE (EPAM,SIS,ULEIS), GOES, IMP-8 (CRNE), SAMPEX, SOHO (LASCO), WIND (EPACT, LEMT)

REFERENCES

Arnaud, M. & Rothenflug, R. 1985, Astron. Astrophys. Suppl. Ser., 60, 425

Arnaud, M. & Raymond, J. 1992, ApJ, 398, 394

Bieber, J. W., et al. 2004, ApJ, 601, L103

Breneman, H. H. & Stone, E. C. 1985, ApJ, 299, L57

Cane, H. V., von Rosenvinge, T. T., Cohen, C. M. S., & Mewaldt, R. A. 2003, Geophys. Res. Lett., 30 (12), 8017

Chen, J., Guzik, T. G., & Wefel, J. P. 1995, ApJ, 442, 875

Cliver, E. W. 2006, ApJ, 639, 1206

Cohen, C. M. S., et al. 1999a, Geophys. Res. Lett., 26, 149

Cohen, C. M. S., et al. 1999b, Geophys. Res. Lett., 26, 2697

Cohen, C. M. S., et al. 2003, Adv. Space Res., 32(12), 2649

Cohen, C. M. S., et al. 2005, J. Geophys. Res., 110, A09S16, doi:10.1029/2005JA011004

Decker, R. B. & Vlahos, L. 1986, ApJ, 306, 710

Dietrich, W. F. & Lopate, C. 1999, Proc. 26th Int. Cosmic Ray Conf. (Salt Lake City), 6, 71

Ellison, D. & Ramaty, R. 1985, ApJ, 298, 400

Forman, M. A. & Webb, G. 1985, in Collisionless Shocks in the Heliosphere: A Tutorial Review, ed. R. G. Stone & B. T. Tsurutani, Geophys. Monongr., 35, 91

Garcia Munoz, M., Mason, G. M., & Simpson, J. A. 1975, ApJ, 201, L145

Giacalone, J. 2005a, ApJ, 624, 767

Giacalone, J. 2005b, ApJ, 628, L37

Gloeckler, G. & Geiss, J. 1998, Space Sci. Rev., 84, 275

Gold, R. E., et al. 1998, Space Sci. Rev., 86, 541

Gopalswamy, N., Lara, A., Kaiser, M. L., & Bougeret, J.-L. 2001, J. Geophys. Res., 106, 25261

Gopalswamy, N., Xie, H., Yashiro, S. & Usoskin, I. 2005, Proc. 29th Int. Cosmic Ray Conf. (Pune) 1, 169

Jokipii, J. R. 1982, ApJ, 255, 716

Jokipii, J. R. 1987, ApJ, 313, 842

Kahler, S. W., Reames, D.V., & Sheeley, N. R., Jr. 2001, ApJ, 562, 558

Kahler, S. W., Simnett, G. M., & Reiner, M. J. 2003, Proc. 28th Int. Cosmic Ray Conf. (Tsukuba), 6, 3301

Klecker, B., et al. 2003, Proc. 28th Int. Cosmic Ray Conf. (Tsukuba), 6, 3277

Klecker, B., et al. 2005, Proc. Solar Wind 11 - SOHO 16 (Whistler, Canada), ESA SP-592, 77

Labrador, A. W., Leske, R. A., Mewaldt, R. A., Stone, E.C., & von Rosenvinge, T. T. 2003, Proc. 28th Int. Cosmic Ray Conf. (Tsukuba), 6, 3269

Labrador, A. W., Leske, R. A., Mewaldt, R. A., Stone, E.C., & von Rosenvinge, T. T. 2005, Proc. 29th Int. Cosmic Ray Conf. (Pune), 1, 99

Laivola, J., Torsti, J., & Kocharov, L. 2003, Proc. 28th Int. Cosmic Ray Conf. (Tsukuba), 6, 3233

Lee, M. A. 2005a, ApJS, 158, 38

Lee, M. A. 2005b, AIP Conference Proc. 781, The Physics of Collisionless Shocks, ed. G. Li, G. P. Zank, & C. T. Russell, (Melville: AIP), 240

Lehtinen, I., Torsti, J., & Mäkelä, P. 2005, Proc. 29th Int. Cosmic Ray Conf. (Pune), 1, 63

Leske, R. A., et al. 2003, AIP Conference Proc 679, Proc. 10th Int. Solar Wind Conf., ed. M. Velli, R. Bruno, & F. Malara, (Melville: AIP), 619

Li, G. & Zank, G. P. 2005, Geophys. Res. Lett., 32, L02101, doi:1029/2004GL021250

Luhn, A., et al. 1984, Adv. Space Res., 4(2), 161

Luhn, A., Klecker, B., Hovestadt, D., & Möbius, E. 1987, ApJ, 317, 951

Mäkelä, P. & Torsti, J. 2001, Sol. Phys., 204, 215

Manchester, W. B., et al. 2005, ApJ, 622, 1225

Mann, G., Jansen, F., MacDowall, R. J., Kaiser, M. L., & Stone, R. G. 1999, A&A, 348, 614

Mann, G., Klassen, A., Aurass, H., & Classen, H.-T. 2003, A&A, 400, 326

Mason, G. M., et al. 1998, Space Sci. Rev., 86, 409

Mason, G. M., Mazur, J. E., & Dwyer, J. R. 1999, ApJ, 525, L133

Mason, G. M., et al. 2002, ApJ, 574, 1039

Mason, G. M., Mazur, J. E., Dwyer, J. R., Jokipii, J. R., Gold, R. E., & Krimigis, S. M. 2004, ApJ, 606, 555

Mazur, J. E. & Mason, G. M. 2001, Eos Trans. AGU, 82(47), Fall Meet. Suppl. Abstract SH31C-03

Mazur, J. E., Mason, G. M., Klecker, B., & McGuire, R. E. 1992, ApJ, 401, 398

McComas, D. J. & Schwadron, N. A. 2006, Geophys. Res. Lett., 33, L04101, doi:1029/2005GL025437

Mewaldt, R. A., et al. 2003, Proc. 28th Int. Cosmic Ray Conf. (Tsukuba), 6, 3313

Mewaldt, R. A., et al. 2005, J. Geophys. Res., 110, A09S18, doi:10.1029/2005JA011038

Meziane, K., Hull, A. J., Hamza, A. M., & Lin, R. P. 2002, J. Geophys. Res., 107, 1243, doi:10.1029/2001JA005012

Möbius, E., et al. 2003, Proc. 28th Int. Cosmic Ray Conf. (Tsukuba), 6, 3273

Ng, C. K., Reames, D. V., & Tylka, A. J. 2003, ApJ, 591, 461

Ostrowski, M. 1991, Mon. Not. R. Astr. Soc., 249, 551

Post, D. E., Jensen, R. V., Tarter, C. B., Grasberger, W. H., & Lokke, W. A. 1977, Atomic Data and Nucl. Data Tables, 20, 397

Reames, D. V. 1995a, Rev. of Geophys., Supplement: U.S. National Report to the International Union of Geodesy and Geophysics, 1991-1994, Part 1: Contributions in Space Science, 585

Reames, D. V. 1995b, Adv. Space Res., 15(7), 41

Reames, D. V. 1998, Space Sci. Rev., 85, 327

Reames, D. V. 1999, Space Sci. Rev., 90, 413

Reames, D. V. 2000, ApJ, 540, L111

Reames, D. V. 2002, ApJ, 571, L63

Reames, D. V. & Ng, C. K. 2004, ApJ, 610, 510

Reames, D. V., Meyer, J. P., & von Rosenvinge, T. T. 1994, ApJS, 90, 649

Reames, D. V., Ng, C. K., & Tylka, A. J. 2001, ApJ, 548, L233

Richardson, I. G., Reames, D. V., Wenzel, K.-P., & Rodriguez-Pacheco, J. 1990, ApJ, 363, L9

Sáiz, A., et al. 2005, Proc. 29th Int. Cosmic Ray Conf. (Pune), 1, 229

Sarris, E. T. & Krimigis, S. M. 1985, ApJ, 298, 676

Steinolfson, R. S. 1984, Sol. Phys., 94, 193

Stone, E. C., et al. 1998, Space Sci. Rev., 86, 357

Torsti, J., Mäkelä, P., Teittinen, M., & Laivola, J. 2000, ApJ, 544, 1169

Torsti, J., Kocharov, L., Laivola, J., Lehtinen, N., Kaiser, M. L., & Reiner, M.J. 2002, ApJ, 573, L59

Torsti, J., Laivola, J., & Kocharov, L. 2003, A&A, 408, L1

Tsurutani, B. T. & Lin, R. P. 1985, J. Geophys. Res., 90, 1

Tylka, A.J. 2001, J. Geophys. Res., 106, 25333

Tylka, A. J. 2005, AIP Conference Proc. 781, The Physics of Collisionless Shocks, ed. G. Li, G. P. Zank, & C. T. Russell, (Melville: AIP), 185

Tylka, A. J. & Dietrich, W. F. 1999, Radiation Measurements, 30, 345

Tylka, A. J. & Lee, M. A. 2006, Spectral and Compositional Characteristics of Gradual and Impulsive Solar Energetic Particle Events, Proc. Chapman Conf. on Energetic Solar Particles and Plasmas, ed. N. Gopalswami, J. Torsti, and R. A. Mewaldt, submitted to AGU Books

Tylka, A. J., Boberg, P. R., McGuire, R. E., Ng, C. K., & Reames, D. V. 2000, AIP Conference Proc. 528, Acceleration and Transport of Energetic Particles in the Heliosphere, ed. R. A. Mewaldt, J. R. Jokipii, M. A. Lee, E. Möbius, & T. H. Zurbuchen, (Melville: AIP), 147

Tylka, A. J., et al. 2001, ApJ, 558, L59

Tylka, A. J., et al. 2002, ApJ, 581, L119

Tylka, A. J., et al. 2003, Proc. 28th Int. Cosmic Ray Conf. (Tsukuba), 6, 3305

Tylka, A. J., et al. 2005, ApJ, 625, 474

Tylka, A. J., Cohen, C. M. S., Dietrich, W. F., Lee, M. A., Maclennan, C. G., Mewaldt, R. A., Ng, C. K., & Reames, D. V. 2006, A comparative study of ion characteristics in the large gradual solar energetic particle events of 2002 April 21 and 2002 August 24, ApJS, in press

von Rosenvinge, T. T., et al. 1995, Space Sci. Rev., 71, 155

Wang, Y.-M., Pick, M., & Mason, G. M. 2006, ApJ, 639, 495

Webb, G. M., Zank, G. P., Ko, C. M., & Donohue, D. J. 1995, ApJ, 453, 178

Wiedenbeck, M. E., et al. 2003, AIP Conference Proc 679, Proc. 10th Int. Solar Wind Conf., ed. M. Velli, R. Bruno, & F. Malara, (Melville: AIP), 652

Yashiro, S., et al. 2004, J. Geophys. Res., 109, A07105, doi:10.1029/2003JA010282

Zank, G. P., Rice, W. K. M., & Wu, C. C. 2000, J. Geophys. Res., 105, 25079

Zank, G. P., Li, G., Florinski, V., Matthaeus, W. H., Webb, G. M., & le Roux, J. A. 2004, J. Geophys. Res., 109, A04107, doi:10.1029/2003JA010301

Zhang, J., Dere, K. P., Howard, R. A., Kundu, M. R., & White, S. M. 2001, ApJ, 559, 452

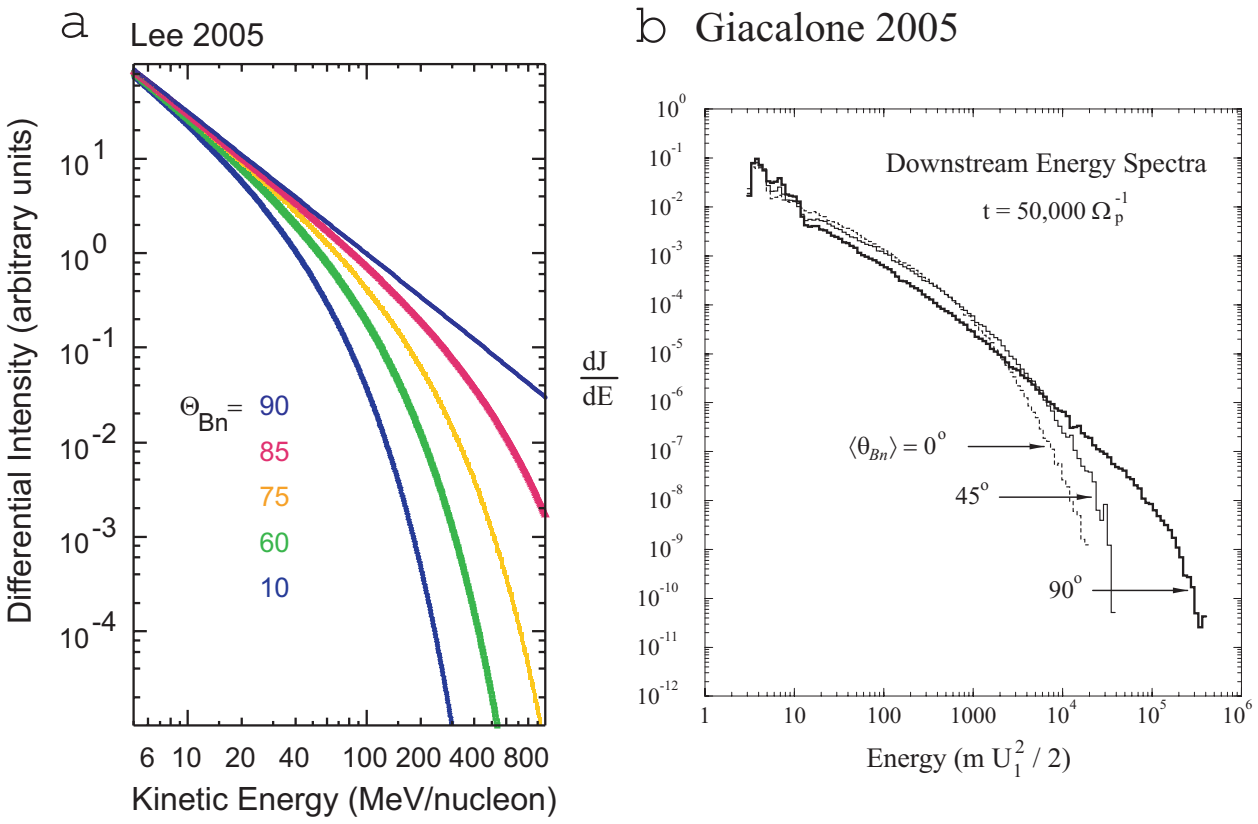

Fig. 1.— Results from two recent theoretical investigations of the effect of the shock-normal angle θ_{Bn} on the spectral shape of the differential proton energy spectrum. The results from Lee (2005a) are based on an analytical derivation of the explicit dependence of the spectrum's e-folding energy on θ_{Bn}. The results from Giacalone (2005a) were produced by time-dependent numerical calculations with three different mean values of θ_{Bn}. Energy is given in terms of the proton mass m and U_1, the upstream in-flow speed in the shock rest frame. For U_1 = 2000 km/s, this energy scale corresponds to ∼20 keV, and the maximum energy in the $< \theta_{Bn} >= 90\,^\circ$ spectrum is ∼6 GeV. The total elapsed time in this calculation is 50,000 Ω_p^{-1}, where Ω_p is the proton cyclotron frequency. This elapsed time corresponds to ∼20 seconds for a typical solar magnetic field of 0.25 G at ∼3 R_S (Gopalswamy et al. 2001; Mann et al. 2003).

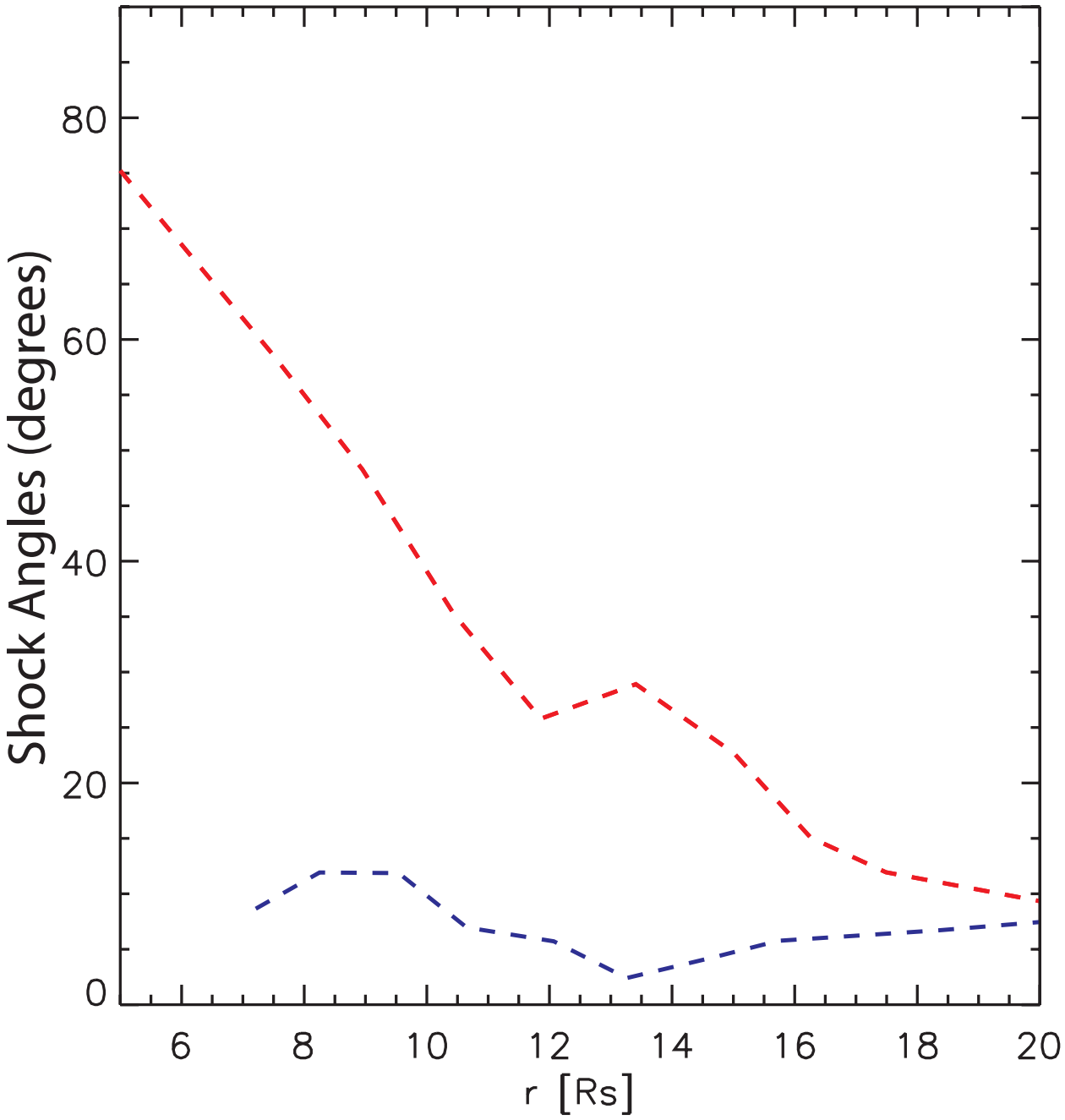

Fig. 2.— Evolution of the shock-normal angle θ_{Bn} along two magnetic flux lines, as derived from a numerical MHD simulation of a ∼1000 km/s CME-driven shock moving outward through the corona. The two flux lines have their footpoints at the same solar longitude but at different solar latitudes. (from Manchester et al. 2005)

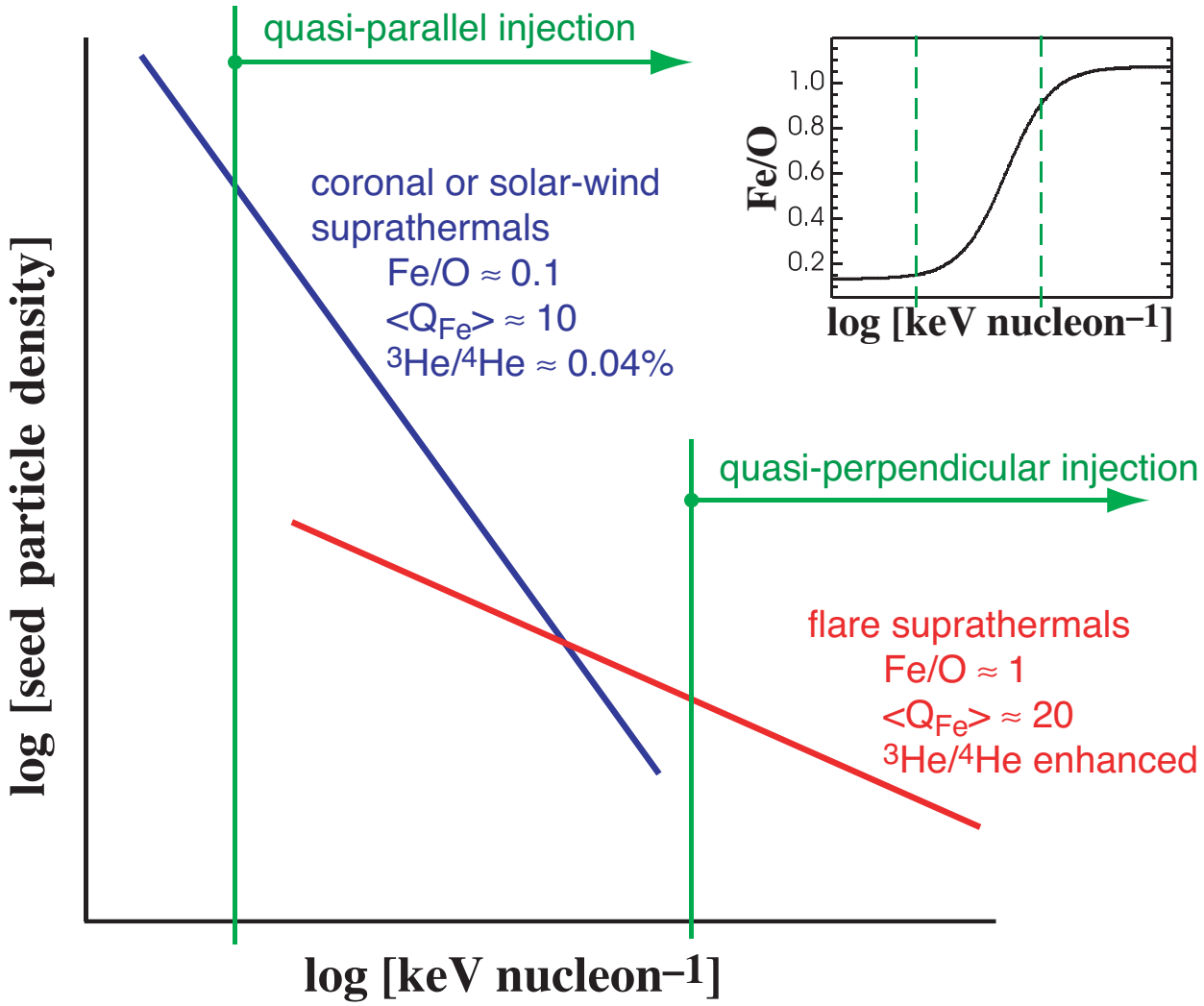

Fig. 3.— A schematic representation of the suprathermal seed population for shock-accelerated solar energetic particles, comprising both coronal (or solar-wind) and flare-accelerated ions. The flare suprathermals are more likely to be apparent in quasi-perpendicular shocks, for which the injection threshold is higher. The inset (upper right) shows how the Fe/O ratio in the seed population changes with energy. As the geometry evolves as the shock moves out from the Sun (generally, from quasi-perpendicular toward quasi-parallel), the composition of the accessible seed population would also change. (from Tylka et al. 2005)

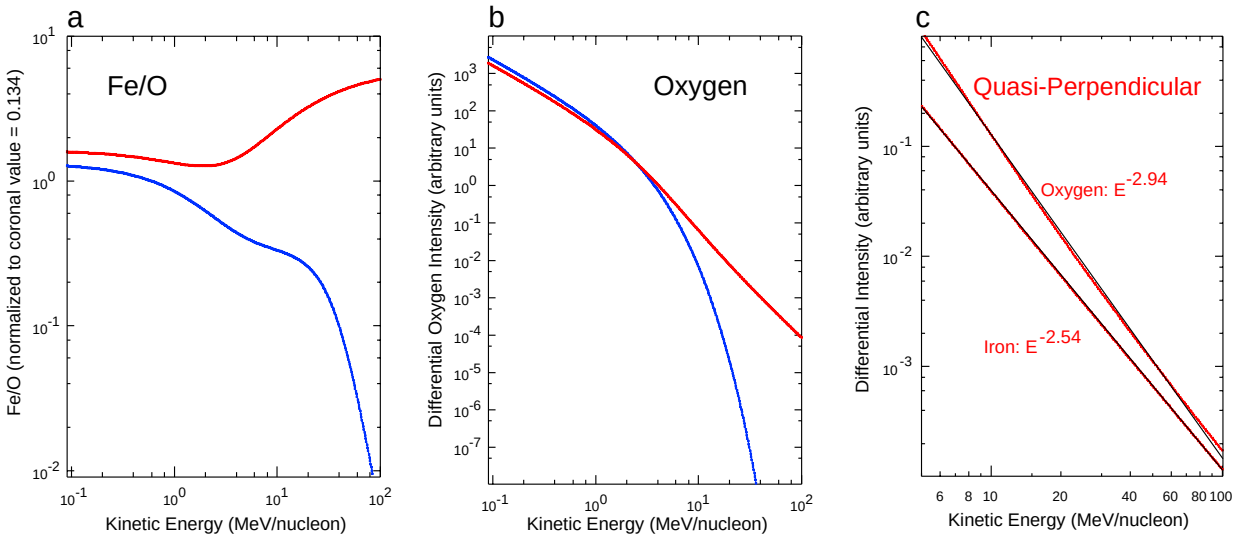

Fig. 4.— Model calculations for (**a**) the Fe/O ratio (normalized to the nominal coronal value) versus energy and (**b**) the differential oxygen spectrum. The model parameters are the same in both cases ($\gamma = 1.5$, $E_0 = 3.0$ MeV/nucleon, and $R = 0.05$) except that the red curves are for the "quasi-perpendicular" case, in which the spectra are averaged over the full range of $0 \leq \theta_{Bn} \leq 90\,^{\circ}$; the blue curves are the "quasi-parallel" case in which $0 \leq \theta_{Bn} \leq 60\,^{\circ}$. Panel (**c**) offers a closer look at the oxygen and iron spectra from the quasi-perpendicular case at 5-100 MeV/nucleon. The black lines are power-law fits to the model calculation. The fitted power-law indices for oxygen and iron are 2.94 and 2.54, respectively.

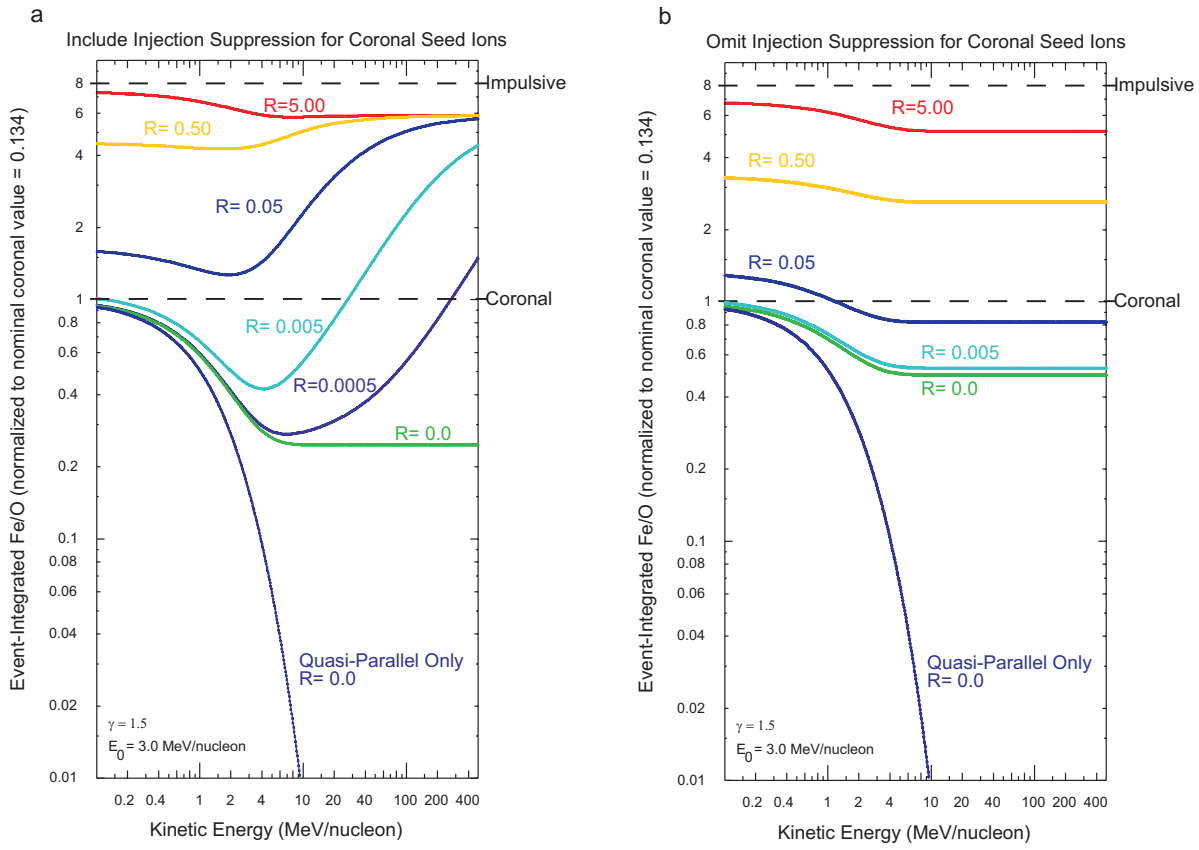

Fig. 5.— Model calculations for the Fe/O ratio (normalized to the nominal coronal value) versus energy. Except for the bottom curve, all of the calculations are for the "quasi-perpendicular" case, in which the spectra are averaged over the full range of $0 \leq \theta_{Bn} \leq 90\,°$; the bottom curve is the "quasi-parallel" case in which $0 \leq \theta_{Bn} \leq 60\,°$. The calculations differ in the relative size of the flare component in the seed population, as specified by the parameter R, defined in equation (9) of the text. The other model parameters are $\gamma = 1.5$ and $E_0 = 3.0$ MeV/nucleon, the same as used in Figure 4. Panel (**a**) shows calculations from this model, in which the injection of ions from the coronal component is suppressed at quasi-perpendicular shocks, according to equation (4). Panel (**b**) shows the same calculations *without* the coronal suppression factor. Panel (**a**) looks like the data; Panel (**b**) does not. See text for further discussion.

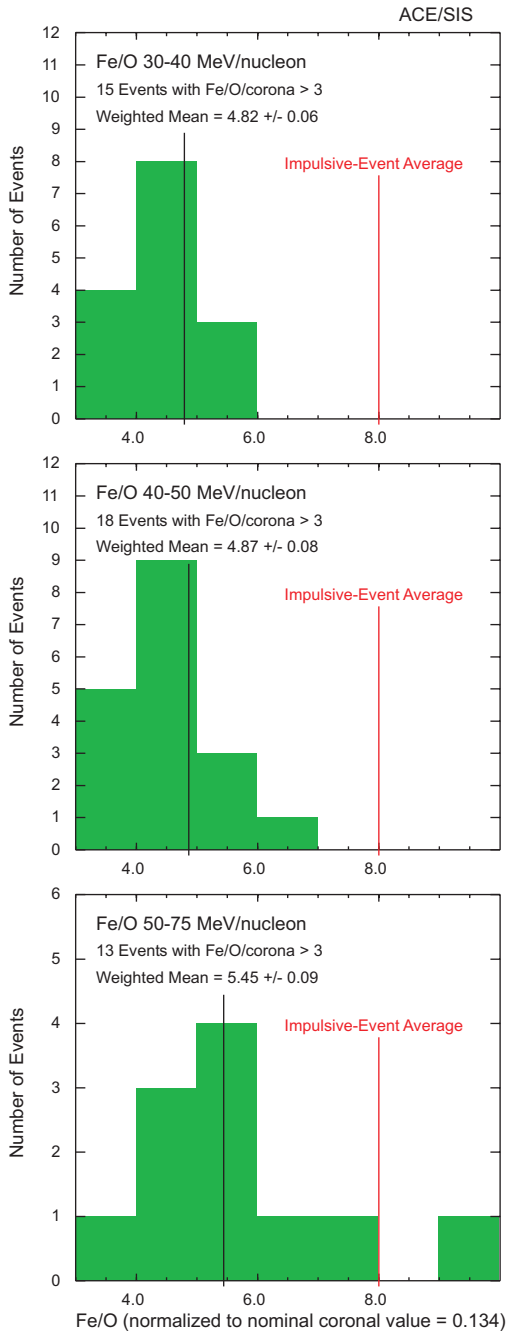

Fig. 6.— Histograms of the Fe/O ratio (normalized to the nominal coronal value) in three energy bins from *ACE*/SIS, based on the event list given in Tylka et al. (2005). In each histogram, only those events in which the Fe/O ratio is at least three times the nominal coronal value are included. Also marked in each panel is the weighted mean of the included events and the average Fe/O value in ^{3}He-rich impulsive events, as given by Reames (1995b). For the highest energy bin (bottom panel), there are two events with large and poorly-determined normalized Fe/O values (12.2 ± 8.6 and 16 ± 7) that are included in calculating the weighted average but are not represented in the histogram. The largest normalized Fe/O value shown in the bottom histogram is also only poorly determined (9.4 ± 5.1).

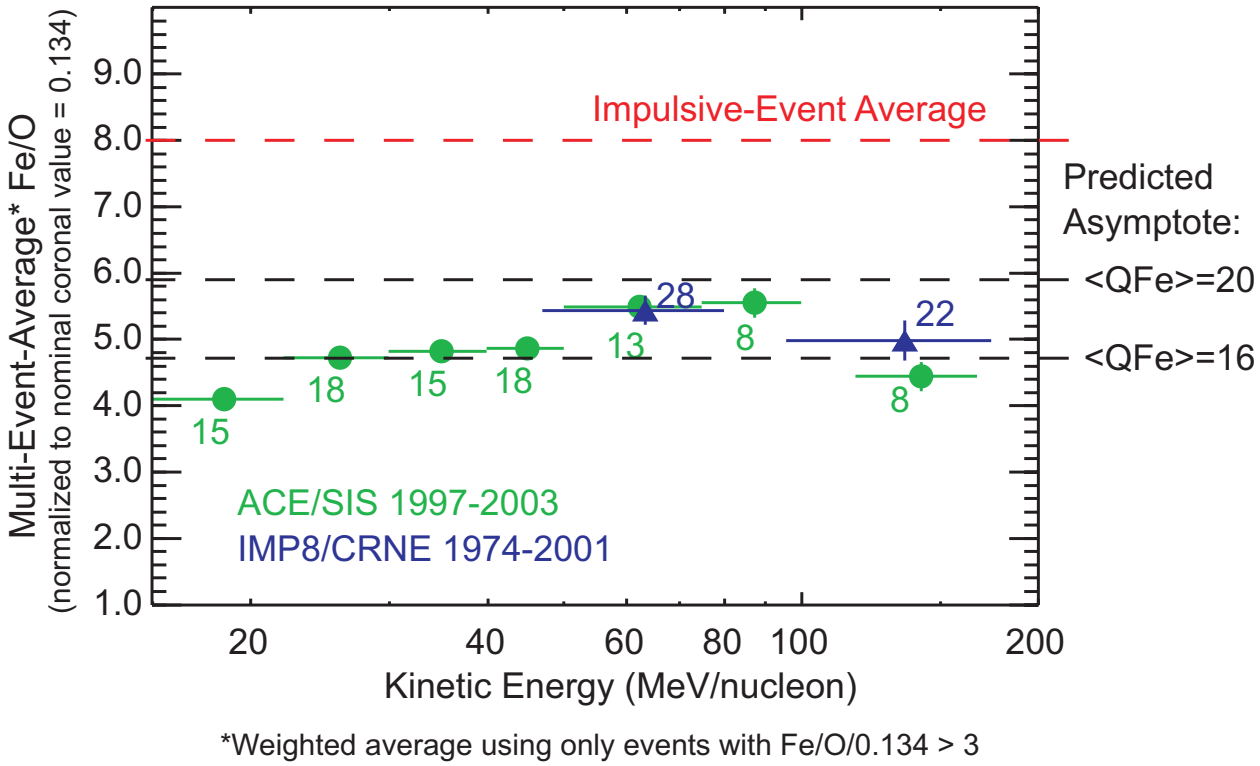

Fig. 7.— Weighted means of Fe/O among Fe-rich events from histograms like those in Figure 6, plotted versus energy. Results from *ACE*/SIS (circles) and *IMP8*/CRNE (triangles) are included; the number beside each point tells how many events contributed to the average. In each energy bin, the average included only those events in which the Fe/O ratio at that energy exceeded three times the nominal coronal value. The dashed red line shows the average Fe/O value in ^{3}He-rich impulsive events (Reames 1995b). The dashed black lines indicate the expected asymptotic value of Fe/O from the model for two reasonable values of $<Q_{Fe}>$. See text for further details.

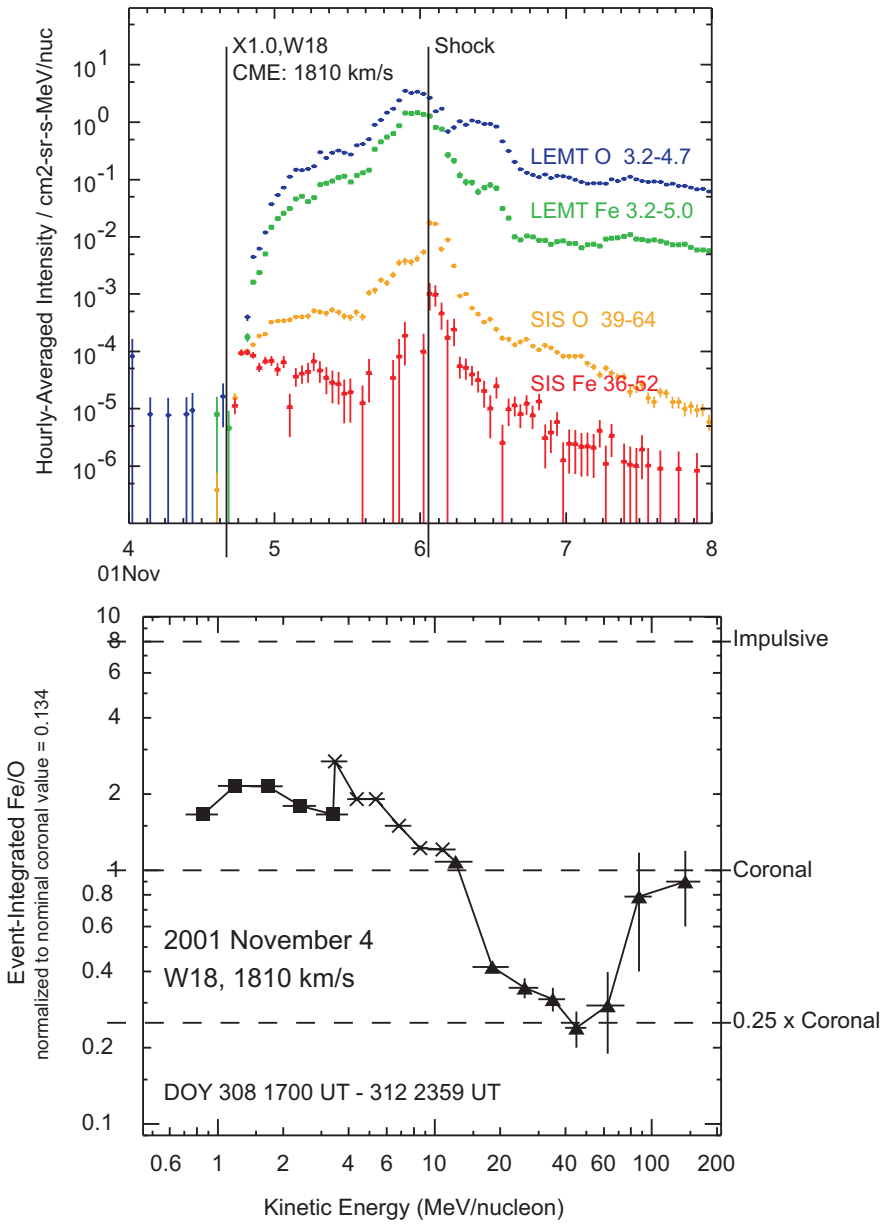

Fig. 8.— Top: Time-intensity profiles of oxygen and iron ions from the Low Energy Matrix Telescope (LEMT; von Rosenvinge et al. 1995) on *Wind* at ∼3 MeV/nucleon and from *ACE*/SIS at ∼40 MeV/nucleon in the solar particle event of 2001 November 4-7. The intensities are largest near the arrival of the quasi-perpendicular shock on 2001 November 6. Bottom: event-integrated Fe/O (normalized to the nominal coronal value) from the Electron Proton Alpha Monitor (EPAM; Gold et al. 1998) on *ACE* (squares), *Wind*/LEMT (crosses), and *ACE*/SIS (triangles) versus energy in this event.

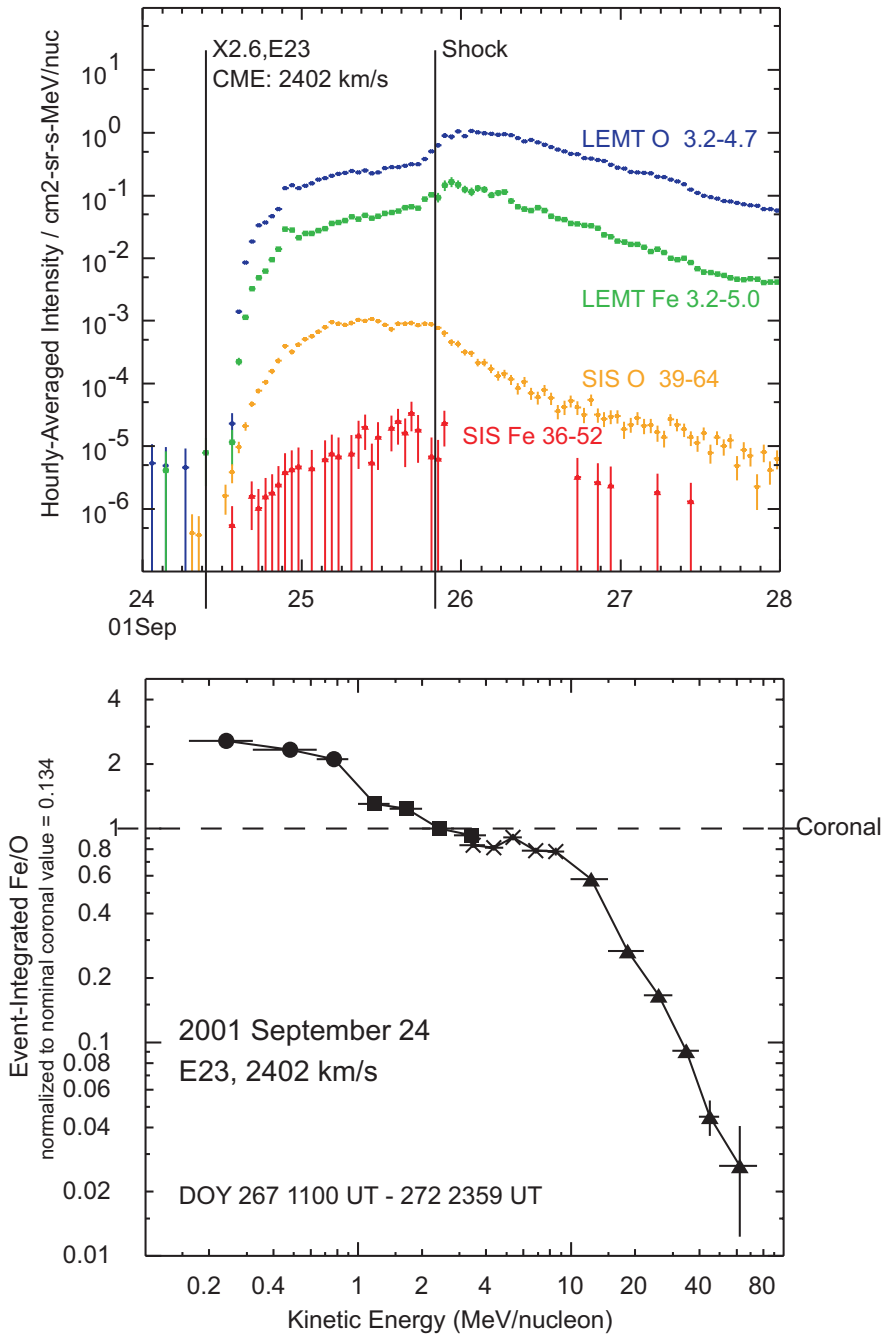

Fig. 9.— Top: Time-intensity profiles of oxygen and iron ions from *Wind*/LEMT at ∼3 MeV/nucleon and from *ACE*/SIS at ∼40 MeV/nucleon in the solar particle event of 2001 September 24-27. Bottom: Event-integrated Fe/O (normalized to the nominal coronal value) from the Ultra Low Energy Isotope Spectrometer (ULEIS; Mason et al. 1998) on *ACE* (circles), *ACE*/EPAM (squares), *Wind*/LEMT (crosses), and *ACE*/SIS (triangles) versus energy in this event.

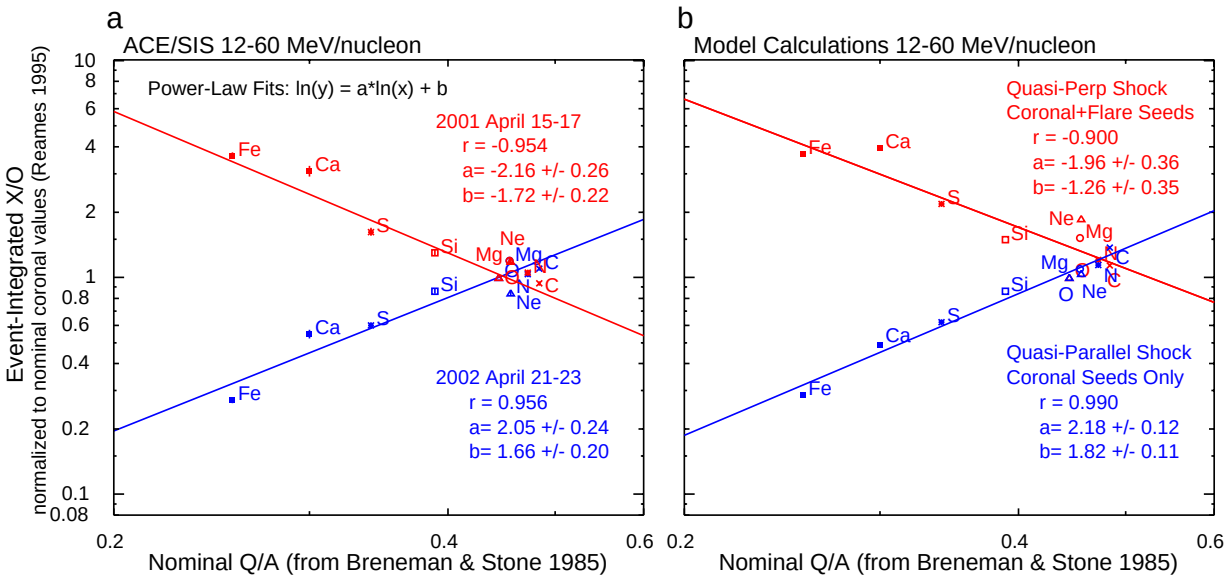

Fig. 10.— (**a**) Breneman & Stone (1985) fractionation at 12-60 MeV/nucleon, as observed by *ACE*/SIS, in the events of 2001 April 15 (in red) and 2002 April 21 (in blue). The relative abundances, normalized to the average abundances in gradual SEP events (as given by Reames 1995b), are roughly organized as power-laws in the nominal Q/A, where the Q values are taken from the averages in a survey of gradual events (Luhn et al. 1984). The parameters a and b for fits to the form $\ln y = a \cdot \ln x + b$ and the correlation coefficient r are noted for both events. (**b**) Model calculations for these two events, using parameters chosen to roughly match the Fe and O spectral shapes above a few MeV/nucleon, as shown in Figures 11. The event in red is modeled as a quasi-perpendicular shock, acting on a seed population containing both coronal and flare ions; the event in blue is modeled as a quasi-parallel shock, acting on a coronal seed population. Like the data, the model results have been fitted to power-laws. To within the uncertainties, the resulting fit parameters are the same as those in the data. The correlation coefficients r are also nearly the same in both the data and model. The *ACE*/SIS data were provided by C.M.S. Cohen.

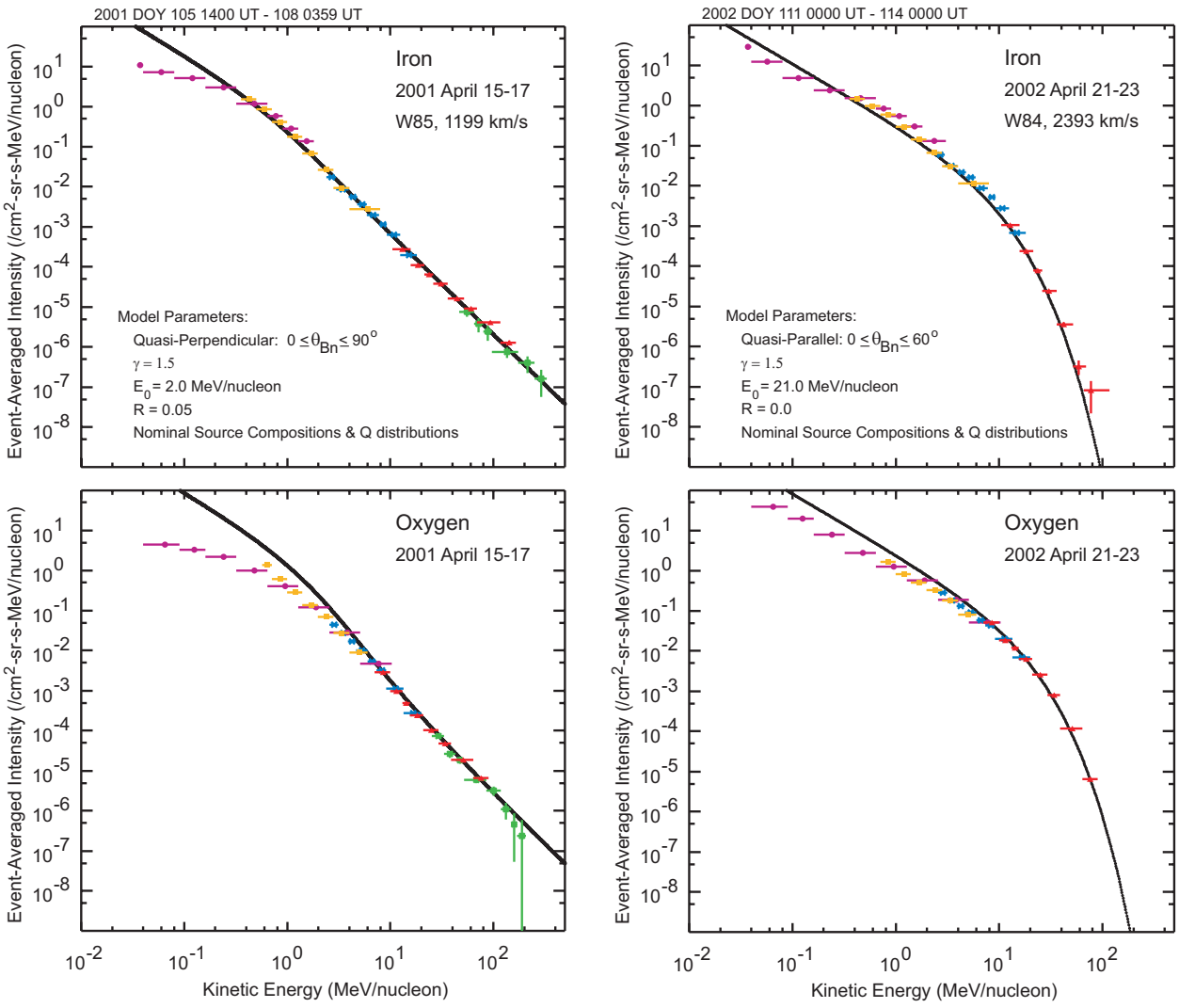

Fig. 11.— Event-averaged spectra for iron (top) and oxygen (bottom) in the events of 2001 April 15 (left) and 2002 April 21 (right). Color and symbol shape distinguish datapoints from (in order of increasing energy) *ACE*/ULEIS, *ACE*/EPAM, *Wind*/LEMT, *ACE*/SIS, and (in the 2001 event) *IMP8*/CRNE. Galactic and anomalous cosmic-ray backgrounds have been subtracted. The black curves are from the model described in Section 3, using the parameters noted on the plots. The model results were normalized to the observed oxygen intensity at 8.4 MeV/nucleon, as determined by the average of measurements from *Wind*/LEMT and *ACE*/SIS; the normalizations for Fe (and other elements; see Figure 10) were then fixed automatically by the model.

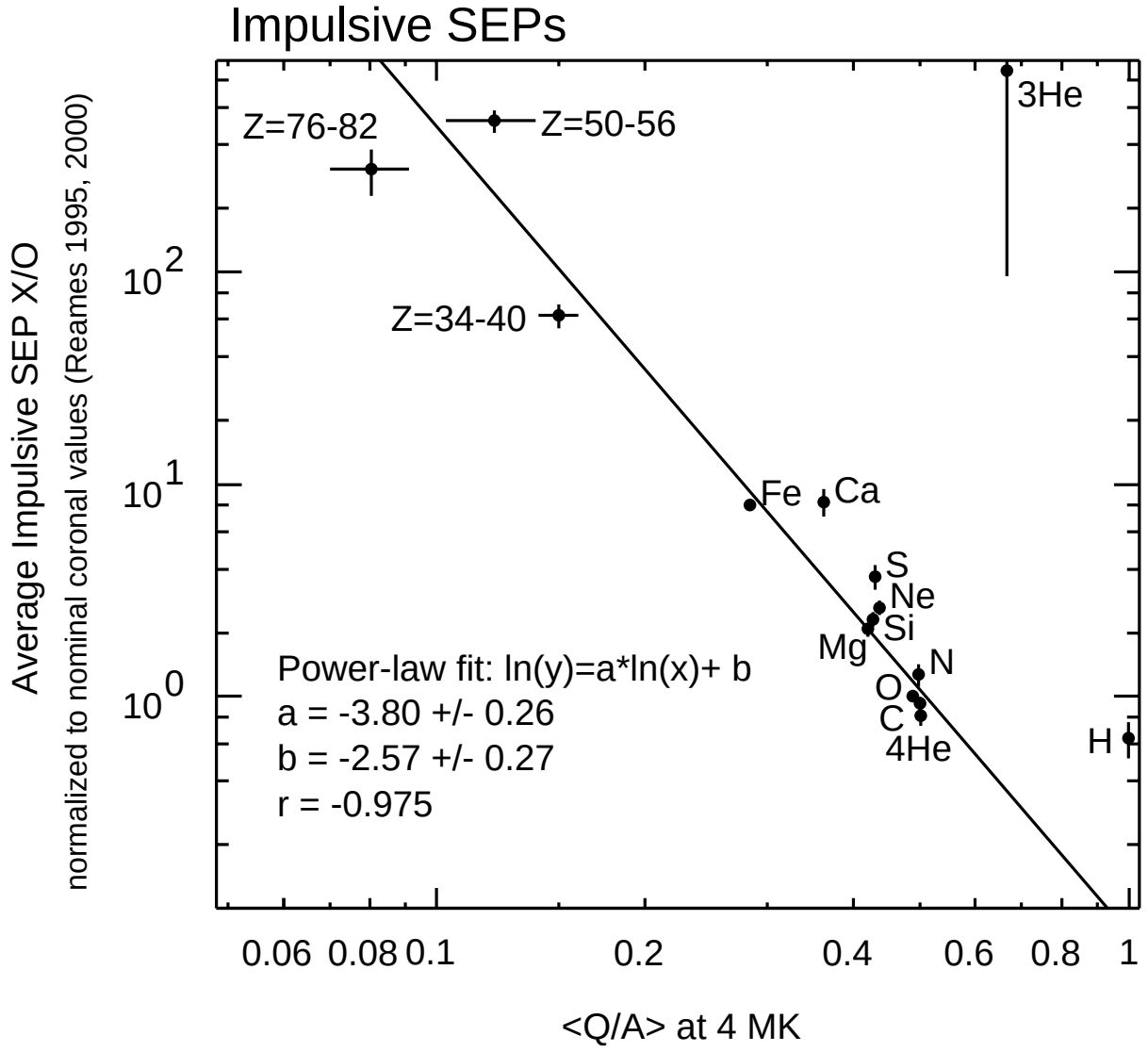

Fig. 12.— Average relative abundances in impulsive SEP events, normalized to nominal coronal values (Reames 1995b; 2000) and plotted versus mean charge-to-mass ($< Q/A >$) values corresponding to a 4.0 MK source temperature. Abundance values are taken from Reames (1995b) and Reames & Ng (2004). The $< Q/A >$ values come from Arnaud & Rothenflug (1985), Arnaud & Raymond (1992, for Fe) and Post et al. (1977, for trans-Fe ions). Also shown is a correlation fit of the form $\ln y = a \cdot \ln x + b$. The fitted slope is $a = -3.80 \pm 0.26$ and the correlation coefficient is $r = -0.975$. This fit did not include the ^{3}He and H datapoints. The fit line is essentially unchanged if the trans-Fe datapoints are also omitted.

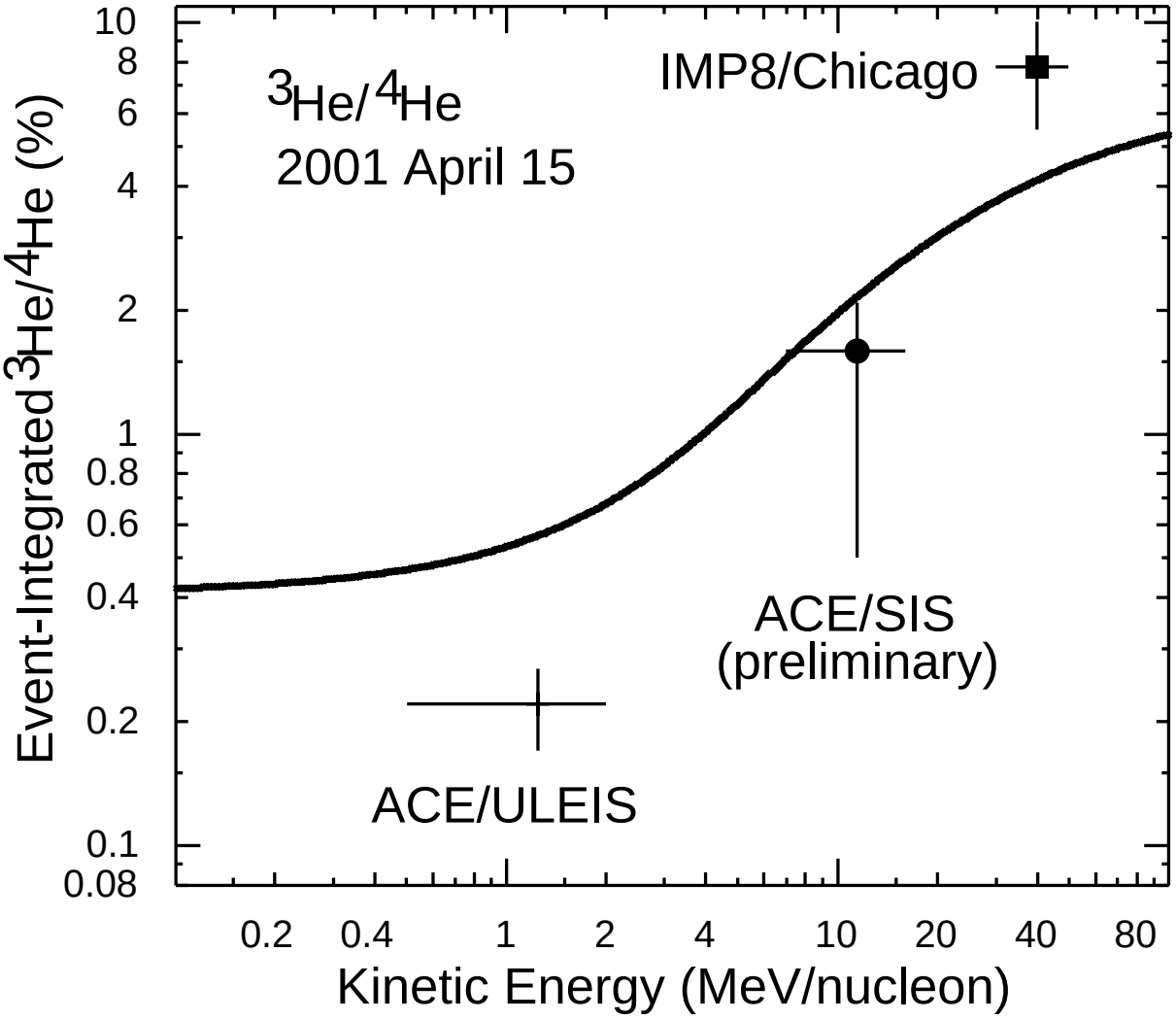

Fig. 13.— Measurements of the ^{3}He/^{4}He ratio at various energies in the 2001 April 15 ground-level event from *ACE* and *IMP8*. The curve is the model calculation, using the same parameters for this event as in Figures 10 and 11. See text for further details. The *ACE*/ULEIS datapoint was previously reported in Tylka et al. (2002). M. Wiedenbeck provided the preliminary result from *ACE*/SIS. W.F. Dietrich provided the *IMP8*/Chicago measurement.

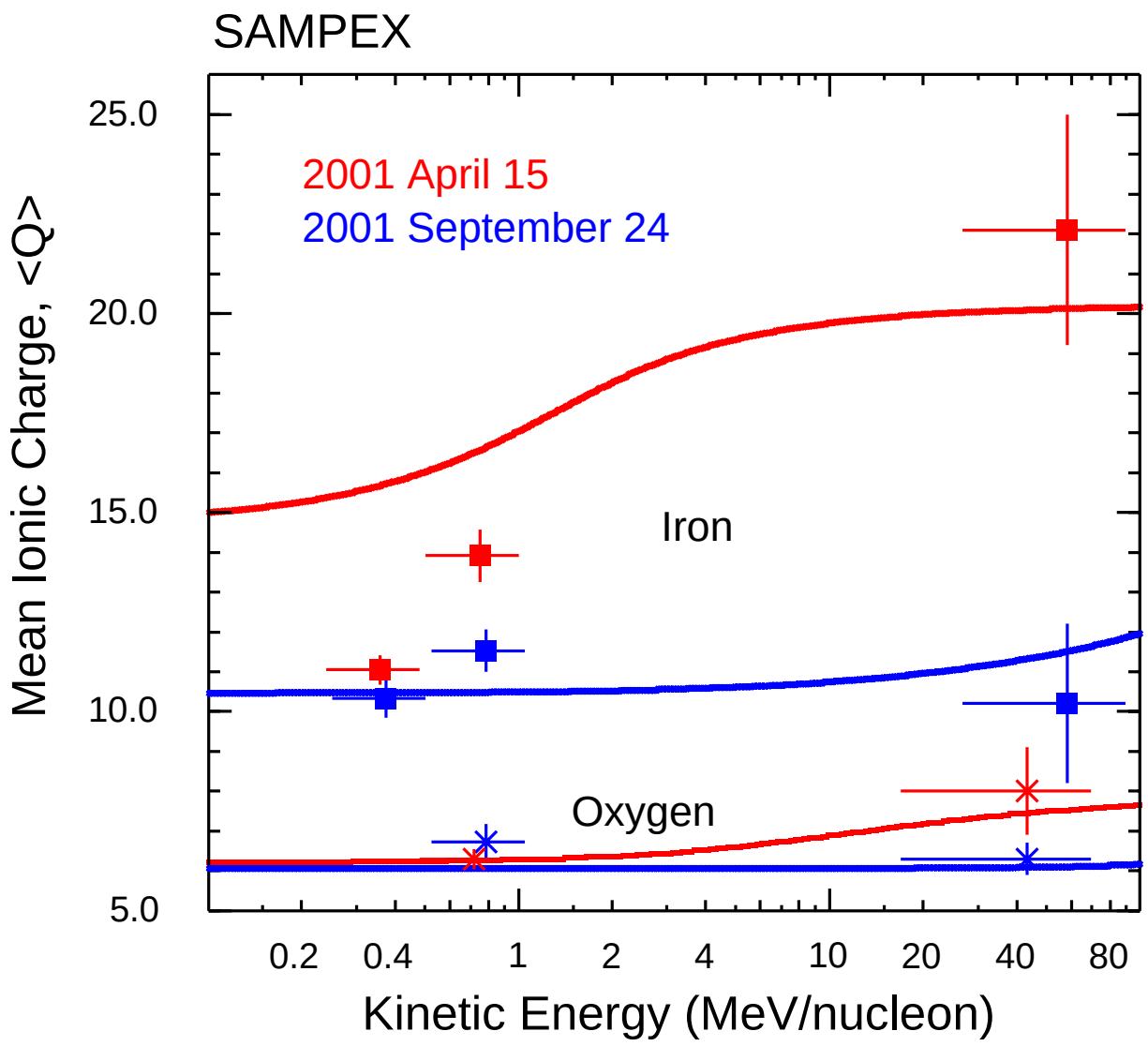

Fig. 14.— Measured charge states from *SAMPEX* (Mazur & Mason 2001; Labrador et al. 2003) for iron (squares) and oxygen (asterisks) versus energy for two events, 2001 April 15 (in red) and 2001 September 24 (in blue). Overlapping datapoints at low energies have been slightly displaced horizontally for clarity. The curves are from the model calculations, as described in the text.